Radiation Fluxes at the FIFE Site

Final Report for Period
January 1, 1991 - July 31, 1992

NASA Grant NAG5-894

by

Elizabeth A. Walter-Shea, Blaine L. Blad, Pedro Zara, Roel Vining,
Cynthia J. Hays and Mark A. Mesarch

Department of Agricultural Meteorology
Institute of Agriculture and Natural resources
University of Nebraska-Lincoln
Lincoln, Nebraska 68583-0728

AgMet Technical Report 93-1
January 1993

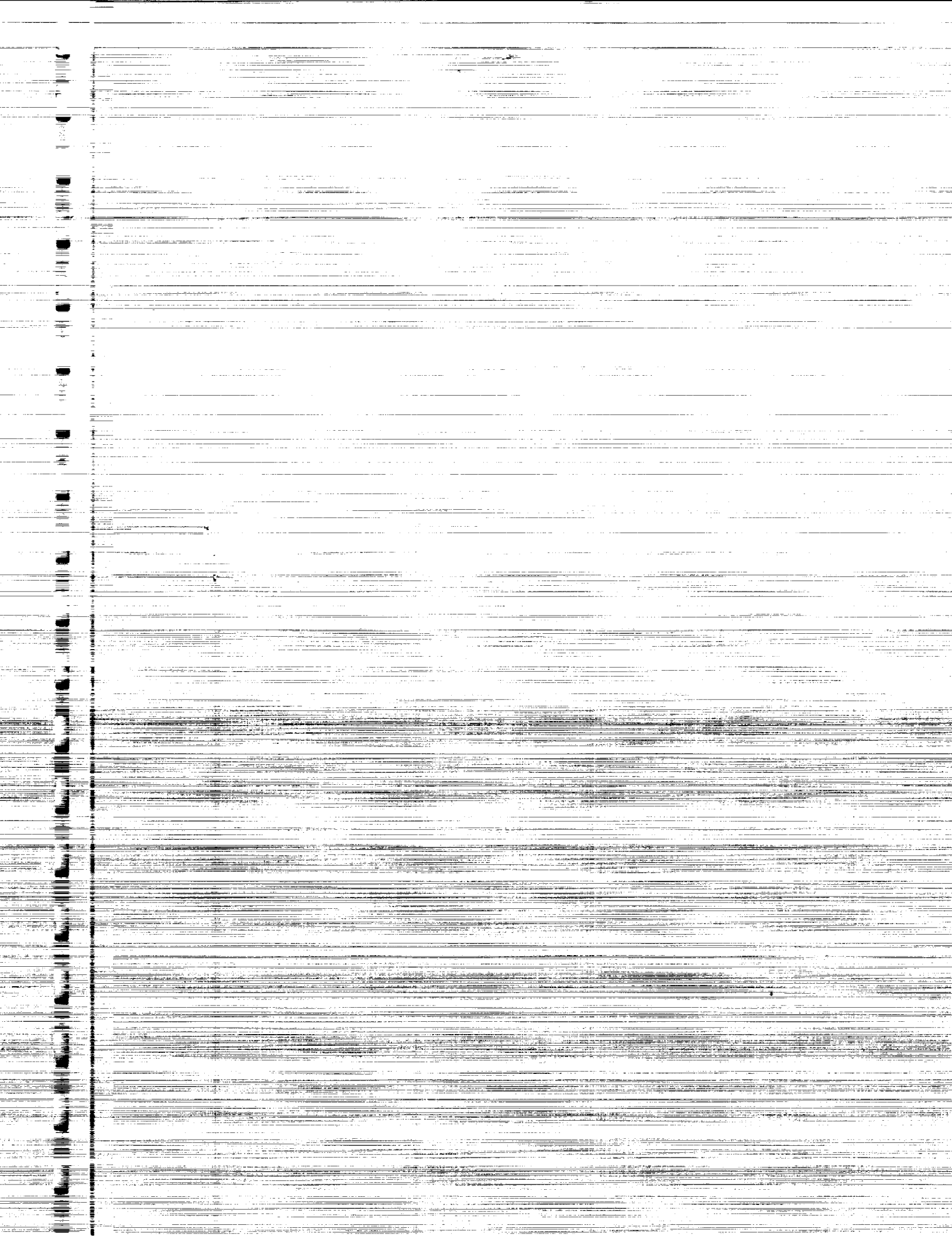

1. INTRODUCTION

The main objective of the International Satellite Land Surface Climatology Project (ISLSCP) has been stated as "the development of techniques that may be applied to satellite observations of the radiation reflected and emitted from the Earth to yield quantitative information concerning land surface climatological conditions." The major field study, FIFE (the First ISLSCP Field Experiment), was conducted in 1987-89 to accomplish this objective. Four intensive field campaigns (IFCs) were carried out in 1987 and one in 1989. Factors contributing to observed reflected radiation from the FIFE site must be understood before the radiation observed by satellites can be used to quantify surface processes. Our last report (Walter-Shea et al., 1992b) focused on slope effects on incoming and outgoing shortwave radiation and net radiation from data collected in 1989. We report here on the final analysis of the slope data as well as results from thermal radiation studies conducted during the FIFE experiment. The specific areas reported are:

1. analysis of slope effects on measured reflectance values and estimates of surface albedo;
2. using remotely-measured surface temperatures as a means of estimating sensible heat flux from the Konza Prairie;
3. extracting canopy temperatures from remotely-measured composite surface temperatures;
4. modelling the measured composite temperature of partially vegetated surfaces;
5. estimating gap distribution in partially vegetated surfaces from reflectance measurements.

2. Slope Effects on Measured Reflectance Values and Surface Albedo Estimates

2.1 Introduction

Topographic variation and distance must be considered to properly characterize incoming solar radiation with *in situ* measurements over regions (Dubayah et al., 1990). The task of characterizing incoming solar radiation in topographic varying regions is difficult because of the necessity of characterizing the topographic relief. Net solar radiation may be even more difficult to describe in topographically varying areas where reflectance may vary spatially. Spatial variability even in areas of gentle topographic relief as at FIFE influence net solar radiation because of the dependence of downwelling irradiance on topography (Dubayah, 1992) and because of the dependence of reflectance on topography, resulting from microclimatic factors. The net shortwave balance has a significant effect on the total radiation balance so that characterizing the shortwave component is critical.

Walter-Shea et al. (1992b), through measurements of upright and inverted Eppley pyranometers mounted horizontally and parallel to the surface, found differences in calculated albedo due to instrument position relative to the surface. The effect differed according to topographic condition, with an average 1% overestimate for North- and West-facing slopes (relative errors of 6 to 7%). However, the reflected radiance (Wm^{-2}) varied little so that the incoming radiation was of most importance. Dubayah (1992) concluded that most of the variability in net solar radiation was caused by topographic modulation of incoming beam and not by changes in reflectance at the FIFE site. Dubayah argues that the grasses stand erect regardless of slope and therefore the reflectance from grasses on leveled and sloped sites will not vary.

Spectral radiant flux densities ($W\ m^{-2}\ sr^{-1}\ \mu m^{-1}$) of sloped and level plots at the FIFE site were normalized to investigate the variation of reflectance factors due to topographic effects. Differences resulting from using actual and effective radiant flux densities as measures of incident radiation for calculating reflectance from sloped surfaces are discussed as well.

The Starks et al. (1991b) method of estimating albedo from remotely-sensed data collected from azimuthal planes different from the solar principal plane and from surfaces of varying slope and vegetative cover was tested. Algorithms were developed and tested with FIFE 87 and 88 data (Blad et al., 1990 and Starks et al., 1991b). The algorithms were independently tested using FIFE 89 sites 906 and 916 data (Walter-Shea et al., 1991). FIFE 89 slope data collected at Site 966 were used to evaluate the applicability of these algorithms on areas of varying topography and in using data collected in azimuthal planes different from the solar principal plane.

2.2 Materials and Methods

Instrumentation and Experimental Site. A Barnes Modular Multiband Radiometer (MMR) 12-1000 and Eppley Precision Spectral Pyranometers (PSPs) were used to collect incoming and reflected radiation over 15 prairie vegetative plots and one bare soil plot at FIFE experimental Site 966 (2437-BBS) in 1989. Plots were selected from hill tops (horizontal surfaces) and from slopes with aspects aligned in the four cardinal directions and in close proximity to each other.

The MMR collects spectral data in eight wavebands ranging from the visible to the thermal infrared. The MMR, set with 15° field of view, was mounted on a portable, inclinable mast three meters above the soil surface producing a target spot size of 0.8m at nadir. The MMR was calibrated in 1989 by Dr. Brian Markham at NASA/Goddard Space Flight Center in Greenbelt, Maryland according to the method of Markham et al. (1988). Bidirectional reflected radiation was measured at seven to eight view zenith angles in the plane parallel to the slope aspect at nadir, 20°, 35° and 50° on either side of nadir and normal to the plot (if it varied from the other viewing directions).

Nadir-viewed MMR data were collected over a horizontally-mounted, calibrated Labsphere molded sintered polytetrafluorethylene-based (Spectralon) reference panel (Labsphere Inc., P.O. Box 70, North Sutton, NH 03260) to estimate incident radiation in each MMR wave band. The panel was calibrated using the Department of Agricultural Meteorology's field-reference panel calibration goniometer (Walter-Shea et al., 1992c) following the field calibration method of Jackson et al. (1987). This method corrects panel reflected radiation data for the panel's non-Lambertian properties. Incoming radiation values were estimated from the panel reflected radiation data using MMR calibration coefficients provided by B. Markham to yield units of spectral radiance (W m^{-2} sr^{-1} μm^{-1}).

A portable A-frame was mounted with one upright-mounted Eppley PSP to measure incoming shortwave radiation on a horizontal surface and two inverted Eppley PSPs to measure reflected shortwave radiation component measurements (one horizontally-mounted, the other mounted parallel to the slope). The inclined PSP was adjusted at each plot to the appropriate angle representing the plot slope aspect.

Due to terrain roughness and equipment restrictions, a limited number of MMR and A-frame measurements were made . Approximately two hours were required to complete an entire run (multidirectional measurements over all plots on all slopes) so that large changes in solar zenith angle often occurred during a single run.

Experimental Procedures. MMR nadir-viewed measurements of the reference panel were taken at the beginning of the measurement run, followed by MMR multi-angle reflected radiation measurements over prairie vegetative and bare-soil plots. Repeated measurements from the A-frame were made in the same plots as the MMR, immediately following or bracketing bidirectional reflected radiation measurements. Nadir-viewed reflected radiation from the reference panel was periodically measured during the run with a final panel reading completing

the sequence of measurements or measured at one minute increments during the run with another MMR.

Incoming radiation received on a horizontal surface was corrected to represent radiation received on an inclined surface. Correction requires the effective (or local) solar zenith angle. The effective solar zenith angle was calculated (from Iqbal, 1983) as:

$$\cos\theta_e = \cos\beta\cos\theta_s + \sin\beta\sin\theta_s\cos(\psi-\gamma) \qquad [1]$$

where:

β = slope of surface (measured from the horizontal)
γ = surface azimuth angle (ranging in value from 0 to $\pm$180 with east = +90 and west = -90)
θ_e = effective solar zenith angle
ψ = solar azimuth
θ_s = solar zenith angle
arccos ($\sin\delta\sin\phi + \cos\delta\cos\phi\cos\omega$)
ω = hour angle
ϕ = geographic latitude
δ = declination angle

Incoming radiation values from the A-frame and MMR nadir-viewed reflected radiation from the field-reference panel were cosine corrected to account for incident radiation received at the sloped surface (values multiplied by the ratio of the cosine of the effective solar zenith angle (θ_e) and the cosine of the solar zenith angle (θ_s), i.e., $\cos\theta_e/\cos\theta_s$). Thus, total incoming radiation was cosine corrected.

Reflected radiances from all surfaces were normalized by the incoming flux on the horizontal as a means of eliminating solar zenith angle effects for comparison purposes (referred to as level and slope reflectance factors, RF_{level} and RF_{slope}). Reflected radiances from sloped surfaces also were normalized by the irradiance on sloped surfaces (corrected for effective solar zenith angle and referred to as effective slope RF, $RF_{slope\ eff}$). We hypothesize that if grasses at the FIFE site grow in the manner described by Dubayah (1992) then the interaction between incoming beam and grass is expected to differ among the grasses growing on the slopes and those on level sites since grasses on sloped surfaces are expected to produce "roughened"

surfaces, rougher than those on level plots (assuming vegetation optical properties and canopy structure are identical). Bright areas on the "roughened" surface are expected when $\theta_e < \theta_s$ and more dark areas on the roughened surface when $\theta_e > \theta_s$.

The method of Starks et al. (1991b) for calculating albedo using remotely-sensed data was tested with the slope data set, collected in azimuthal directions according to cardinal directions of N-S and E-W. These azimuthal planes did not always coincide with the solar principal plane.

2.3 Results and Discussion

Slope Effects. We hypothesize that in situations where the effective solar zenith angle, θ_e, illuminating a sloped surface is smaller than the actual solar zenith angle, θ_s (illuminating a level surface) more of the tops of the grasses on the sloped surfaces is expected to be illuminated than on the level surfaces (Fig. 2.1a). Under this situation a higher radiative flux density in the visible portion of the spectrum comes from sloped surfaces than from level surfaces. Also, shadows cast by grasses on sloped surfaces are expected to be shorter than those cast by grasses on level surfaces (Fig. 2.1b) which should result in a higher radiant flux density in the visible portion of the spectrum from sloped surfaces than from level surfaces. Shadows are also expected to play a similar role in the near-infrared (NIR) portion of the spectrum. Smaller shadows cast on the substrate (lower in reflectance than grass surfaces) on the sloped sites (more sunlit areas) will cause a lower NIR reflectance energy than from the level sites. Thus, when $\theta_e < \theta_s$, RF_{slope} are expected to be higher than RF_{level} in the visible and less than in the NIR. $RF_{slope\ eff}$ will be lower than RF_{slope} and possibly closer in value to RF_{level} when θ_e is smaller than θ_s. The opposite would be true for surfaces where θ_e is larger than θ_s.

There is a trend for level and slope RFs to differ as expected, indicating differences in canopy reflectance variability with topography (Fig. 2.2 and Table 2.1), however these differences are small (1% and 4% absolute in the visible and NIR, respectively).

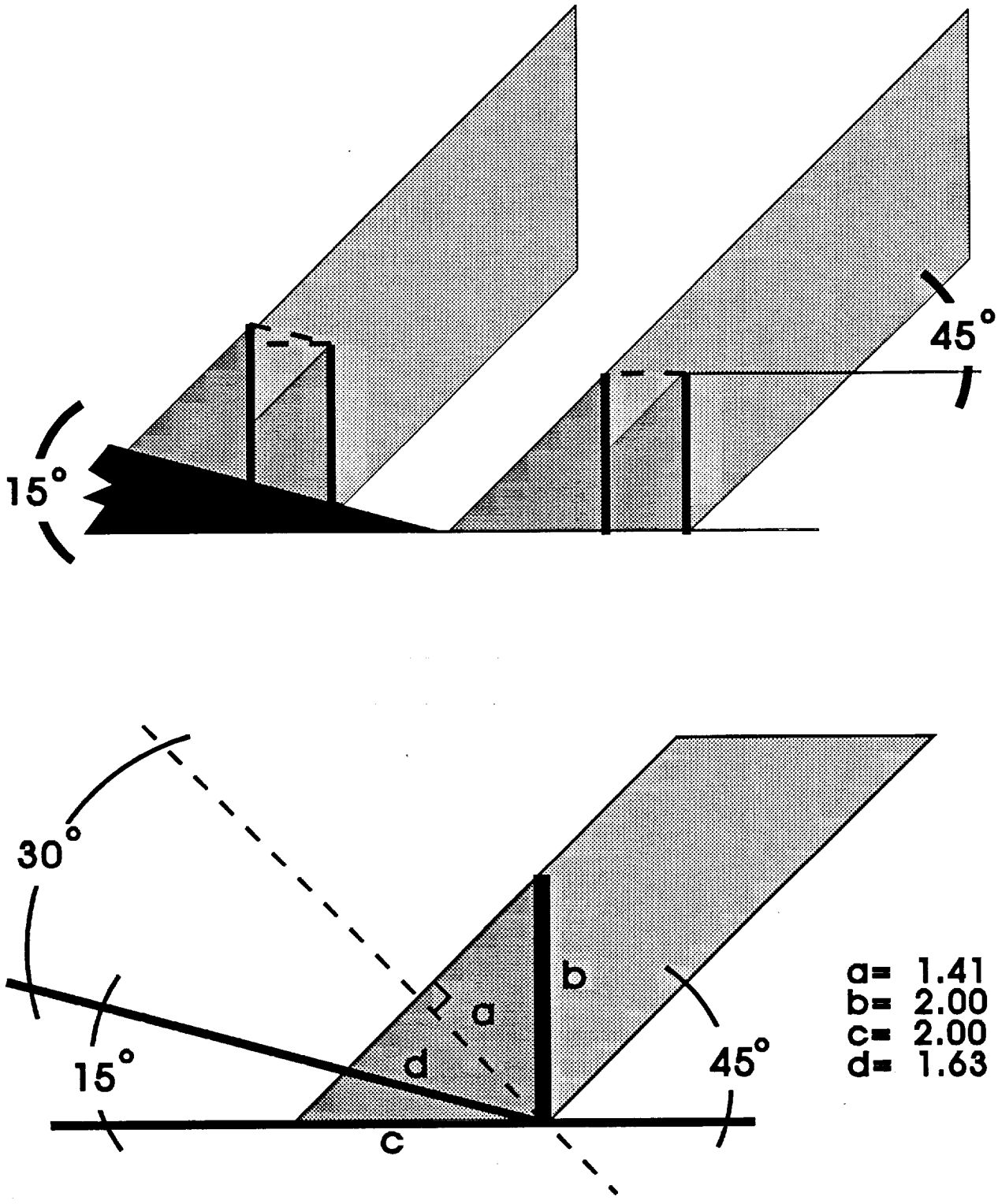

Fig. 2.1. (a) Schematic representing erect grasses on a 15° sloped surface and a level surface illuminated at a 45° solar elevation angle. Shadows cast by grasses on the sloped surface are shorter and the sunlit grass area is greater than on the level slope. (b) Detail of shadow cast by erect grass on the horizontal **c** and on the 15° sloped surface **d**. Length of **c** is greater than **d**.

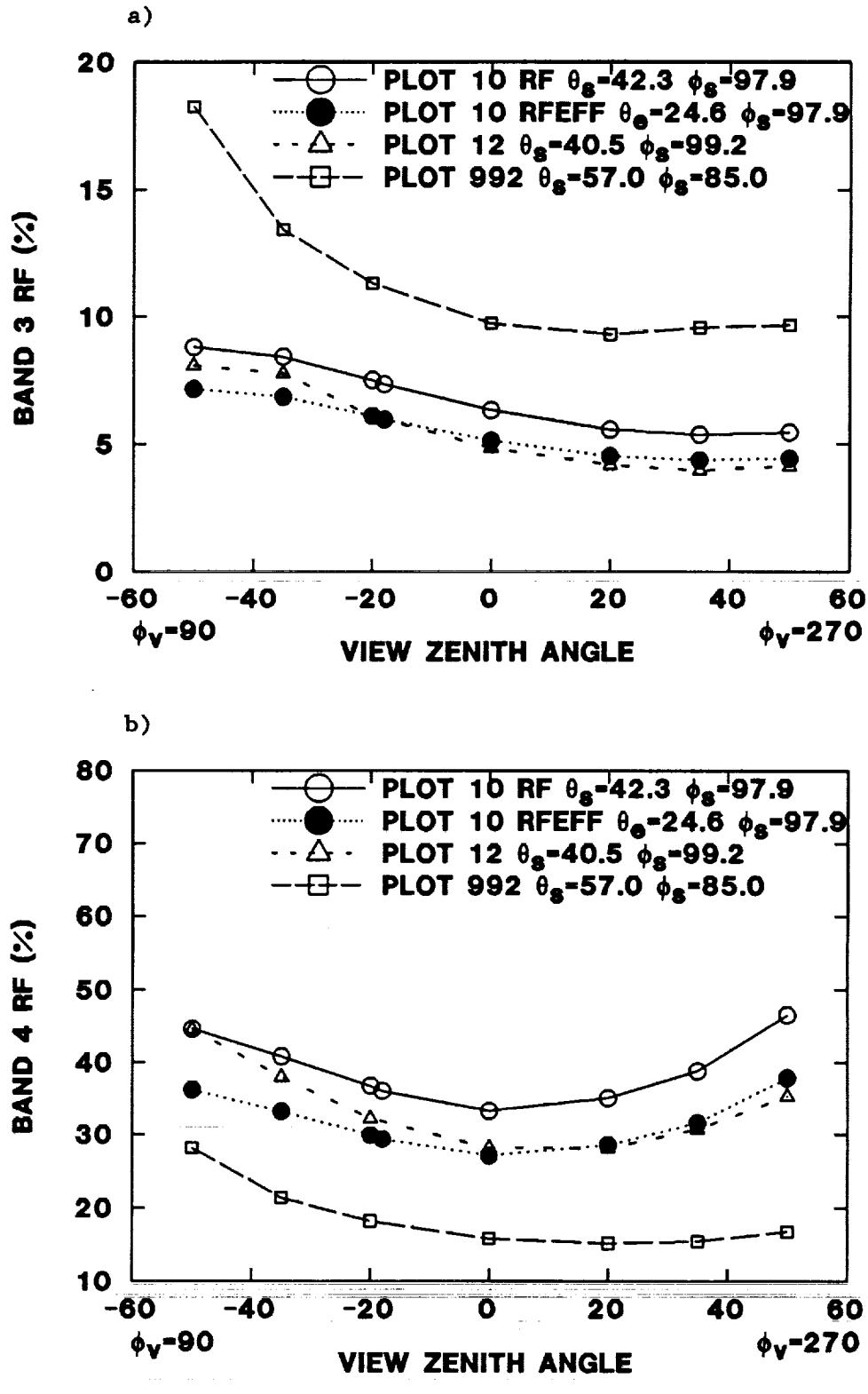

Fig. 2.2 Bidirectional reflectance factors for sloped (Plot 10), level (Plot 12) and bare soil surfaces (Plot 992) at Site 966 for: (a) the red (band 3) and (b) the near-infrared (band 4) portions of the spectrum. θ_s and ϕ_s are the solar zenith and azimuth angles and ϕ_v is the view azimuth angle.

Table 2.1 **Mean bias error and mean relative error between level and slope surface reflectance factors under conditions where the effective solar zenith angle varied from the actual solar zenith angle.**

	No. plots	LAI difference	VISIBLE		NIR	
			MBE	MRE	MBE	MRE
$\theta_e > \theta_s$	45	±2.0	-0.184	-0.030	3.151	0.089
$\theta_e < \theta_s$	25	±2.0	-1.308	-0.228	0.355	0.003
$\theta_e > \theta_s$	34	±0.5	0.203	-0.032	3.667	0.102
$\theta_e < \theta_s$	20	±0.5	-1.321	-0.222	-0.166	-0.013
$\theta_e > \theta_s$	15	±0.25	0.013	0.004	4.087	0.105
$\theta_e < \theta_s$	9	±0.25	-1.603	-0.272	1.673	0.046

Various factors may be contributing to the observed differences including illumination differences (as depicted in Fig. 2.1), species differences, vegetative cover, LAI and background differences.

Albedo Estimates. MMR bidirectionally reflected radiation from plots in various slopes was obtained for a total of 96 cases in 1989 (86 over grass covered surfaces and 10 over a bare soil surface). The algorithms reported in Blad et al. (1990), Walter-Shea et al. (1991) and Starks et al. (1991b) were used to estimate reflected and incoming components of the radiation balance from which albedo estimates were calculated. The data represent variation in plots, solar zenith angle and vegetation characteristics.

Reflected and incident shortwave component estimates and albedo estimates from the various sloped surfaces are compared to measured Eppley PSP component values (Fig. 2.3). Statistical analyses indicate incoming solar radiation estimates agreed well with measured values over all cases with a d-statistic of 0.98 (see Blad et al., 1990 for explanation of the statistics) (Table 2.2).

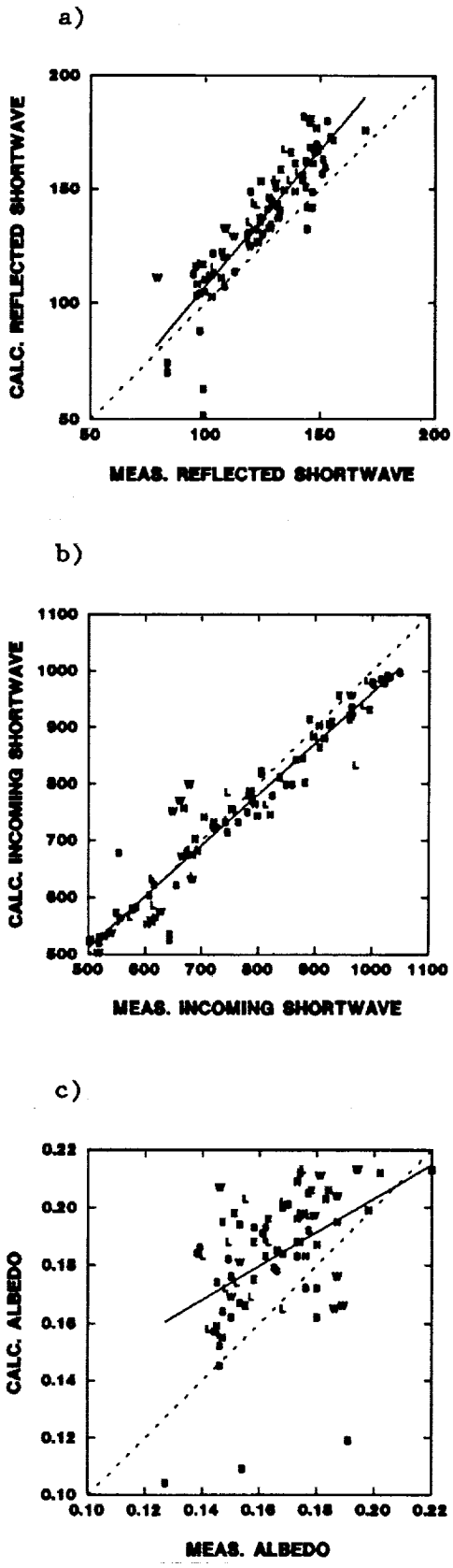

Fig. 2.3 Comparison between Eppley PSP shortwave components and estimated shortwave components (in Wm^{-2}) from FIFE-89 remotely sensed bidirectional reflected radiance data collected at Site 966. Diagonal dashed line represents 1:1 line. Solid line is a fitted regression line. Letter symbols represent as follows: B is the bare soil plot; L, N, S, E, W are vegetated plots which are on level, north-, south-, east-, and west-facing slopes, respectively.

Table 2.2. **Statistics from comparison of estimated incoming shortwave component (using the method of Starks et al. (1991b) with measured values. Input and validation data are from the FIFE 89 slope dataset.**

Component	d	r	r^2	MBE Wm^{-2}	MRE %	RMSE Wm^{-2}	Eu Wm^{-2}	Es Wm^{-2}	x Wm^{-2}	s
all grass	0.98	0.97	0.94	-14.3	-1.5	55.8	53.0	17.6	748.4	147.4
measured									759.7	160.3

where:

d = $1 - [\Sigma(E_i-M_i)^2/\Sigma(|E_i-M|+|M_i-M|)^2]$
E_i = estimated value at time i
M_i = measured value at time i
M = mean measured value for the data set
RMSE = Root Mean Square Error
= $[(N^{-1}\Sigma(P_{ri}-M_i)^2] + ([N^{-1}\Sigma(P_{ri}-E_i)^2])^{1/2}$
E_e = $(N^{-1}\Sigma(P_{ri}-M_i)^2)^{1/2}$
E_u = $(N^{-1}\Sigma(P_{ri}-E_i)^2)^{1/2}$
P_{ri} = predicted value using values derived from least squares regression of estimated and measured values
= $aM_i + b$
a = slope
b = intercept
MBE = Mean Bias Error
= $N^{-1}\Sigma(E_i-M_i)$
MRE = Mean Relative Error
= $N^{-1}[\Sigma(E_i-M_i)/M_i][100]$
x = mean
= $N^{-1}\Sigma V_i$
V_i = estimated or measured values
s = standard deviation
= $[(N-1)^{-1}\Sigma(V_i-x)^2]^{1/2}$

According to the MBE statistic, the model underestimated the measured incoming solar radiation by approximately 14 W m^{-2}; the MRE indicates the underestimate is approximately 1.5% of the measured value. Measured and model means are comparable. The RMSE is approximately 56 W m^{-2} for the model. The agreement between estimated and measured values is not as good as that reported by Walter-Shea et al. (1991), comparing data collected in 1989 but at Site 906 and 916 (with MBE of 4 Wm^{-2} and MREs of 0.04%). Differences may be due to the number of cases used. Only 86 cases were used for the sloped data and approximately 155 cases for Sites

906 and 916. Also, incoming shortwave measurements on Day 166 were not coincident with MMR measurements as was in previous reports.

The reflected component is overestimated in all cases except in the bare soil plots. The overestimates ranged from 12-21 Wm^{-2} (approximately 9-16% of the measured values). These values are slightly better than those achieved over plots reported by Walter-Shea et al., 1991 (MBE of approximately 23 W m^{-2} which is approximately 19% of the measured values), even though the alignment in azimuths was in a plane other than the solar principal plane. Bare soil reflected radiation was underestimated by approximately 13 Wm^{-2}. Nadir-viewed reflected estimates of reflected radiant flux density agreed well and often better than the estimates obtained using the Starks et al. method. Previous tests did not indicate a significant better estimate using nadir-viewed data (Starks et al., 1991a).

The Starks et al. method of estimating albedo did not perform as well as under previous conditions (Table 2.3) (see Walter-Shea et al., 1991). The model performed poorly for plots on the south- and west-facing slopes and the bare soil plots. Previous test of the algorithm using bare soil plots indicate a similar poor performance for bare soil conditions (Starks et al., 1991a).

Table 2.3 **Statistics from comparison of estimated reflected shortwave component (using the method of Starks et al. and normal-viewed values) with measured values. Input and validation data are from the FIFE 89 slope dataset.**

Component	d	r	r^2	MBE Wm^{-2}	MRE %	RMSE Wm^{-2}	Eu Wm^{-2}	Es Wm^{-2}	x Wm^{-2}	s
all grass-S*	0.83	0.92	0.85	15.3	12.1	31.8	29.1	12.7	143.3	21.7
all grass-n	0.89	0.88	0.78	-5.1	-4.7	21.2	19.6	7.9	123.3	27.5
measured									127.4	18.4
level-S	0.80	0.94	0.88	16.2	13.0	33.3	30.4	13.6	142.9	19.5
level-n	0.89	0.85	0.72	0.6	0.2	16.8	15.5	6.5	127.5	23.8
measured									125.4	16.7
north-S	0.88	0.94	0.89	11.9	9.2	25.3	23.2	10.1	139.4	21.7
north-n	0.88	0.95	0.90	-11.7	-10.0	25.7	23.8	9.8	115.8	24.8
measured									127.5	18.1
south-S	0.84	0.91	0.82	14.3	11.2	30.1	27.8	11.7	141.9	24.2
south-n	0.91	0.90	0.80	-1.2	-1.7	20.0	18.5	7.5	126.4	28.8
measured									127.5	19.5
east-S	0.73	0.93	0.87	21.1	15.6	43.1	39.3	17.6	157.9	20.9
east-n	0.92	0.96	0.93	-5.6	-5.2	21.5	20.0	7.7	131.2	29.2
measured									136.8	18.5
west-S	0.79	0.89	0.80	14.5	12.8	32.0	28.9	13.6	136.3	17.9
west-n	0.83	0.80	0.65	-7.1	-6.4	25.1	23.4	9.1	116.9	31.5
measured									119.8	17.5
bare soil-S	0.89	0.91	0.82	-12.6	-12.6	31.8	29.4	12.0	101.4	36.9
bare soil-n	0.84	0.92	0.85	-15.9	-17.5	43.3	40.7	14.8	98.2	47.5
measured									114.1	27.4

* -S represents values obtained using the Starks et al. (1991b) method
-n represents values obtained using normal-viewed values

2.4 Summary and Conclusions

Reflectance factors tend to differ between sloped and leveled surfaces. Although various factors probably contribute to this (including species differences, vegetative cover and background cover), we feel that surface roughness and thus shadows may play an important role.

More studies under controlled conditions are needed to find the significance of surface roughness on reflectances from sloped grass-cover surfaces.

The incoming shortwave component was underestimated on the average by 14 Wm^{-2} (compared to 4 Wm^{-2} in previous studies). The reflected shortwave component was overestimated by about the same magnitude as in previous studies, even though reflected radiation was measured in an azimuthal plane other than the solar principal plane. Albedo estimates were in poor agreement with measured values (10-17% MRE) compared to 4% MRE with FIFE 87-89 level sites. Large errors in incoming and reflected shortwave components contributed to the general overestimate of albedo. The cosine correction to the total incoming shortwave and the lack of coincident measurement of Eppley PSP with the MMR may be factors contributing to the overestimate. Bare soil albedos were greatly underestimated. Nadir derived estimates were in better agreement but often underestimated the measured value.

3. Estimation of Sensible Heat Flux From Remotely-Sensed Canopy Temperatures

3.1 Introduction

The energy balance at the Earth's surface, neglecting energy used for photosynthesis and small miscellaneous processes, is represented by

$$R_n + H + \lambda + G = 0 , \tag{1}$$

where R_n is net radiation, H is sensible heat flux, λ is latent heat flux, and G is soil heat flux. When vegetation covers most or all of the soil, $G \approx 0$ and can be neglected [Brunel, 1989).

Jackson et al. (1985) and Starks et al. (1991b) give procedures for estimating R_n using remotely-sensed multispectral and ground-based meteorological data. Sensible heat flux can be calculated directly with eddy correlation techniques (Kanemasu et al., 1979), or with methods that utilize the temperature gradient between the surface and the air and a measure of the resistance of the atmosphere to heat transfer (Hatfield et al., 1984a; Choudhury et al., 1986; Huband and Monteith, 1986b; Kustas et al., 1989; Brunel, 1989). The latter approach requires measurements of surface temperature.

Surface temperature can be measured with an infrared thermometer (IRT). Temperatures measured- with an IRT generally vary with the view angle of the instrument (Fuchs et al., 1967; Nielsen et al., 1984; Huband and Monteith, 1986a; Zara, 1992). Kimes et al. (1980) found IRT measured temperatures of a wheat canopy can vary by as much as 13°C depending on the view zenith angle. Huband and Monteith (1986a) noted that the influence of solar position and ground cover on canopy temperatures can be minimized by taking measurements at view angles other than nadir.

The primary objective of the research reported here is to determine the optimum view zenith angle, or angles, to measure surface temperatures for accurately estimating H.

3.2 Materials and Methods

Canopy temperatures were measured concurrently with sensible heat fluxes at the First International Satellite Land Surface Climatology Project (ISLSCP) Field Experiment (FIFE) sites 916 (4439-ECV) and 906 (2133-ECA). The vegetation at these sites was a mixture of native grasses, with canopy heights ranging from about 0.20 to 0.85 m.

Surface temperatures were measured with four Everest 4000 Transducer-Multiplexer Infrared Thermometers mounted so that each IRT viewed the same surface area at a view zenith angle of 0° (nadir), 20°, 40°, or 60° (Fig. 3.1). The arc on which the IRTs were mounted pivoted around the nadir position, so the view azimuth angle could be adjusted to any desired angle. Measurements were taken at azimuth intervals of 45°. With this design, an entire set of measurements across the four view zenith angles and the eight view azimuth angles could be taken in approximately 5 minutes.

Each IRT was calibrated before and after the experiment in controlled ambient air temperature conditions, using a blackbody source with variable temperature output values. Each IRT was also checked periodically during each data collection period with a portable blackbody source to make certain it was working properly.

Radiative temperature (T_r) was adjusted for emissivity and reflected longwave radiation to give actual canopy temperature (T_c) using the equation

$$T_c = \{ [R_{bc} - (1 - \epsilon_c)\ B^*] / (\epsilon_c\ \sigma) \}^{0.25} \qquad (2)$$

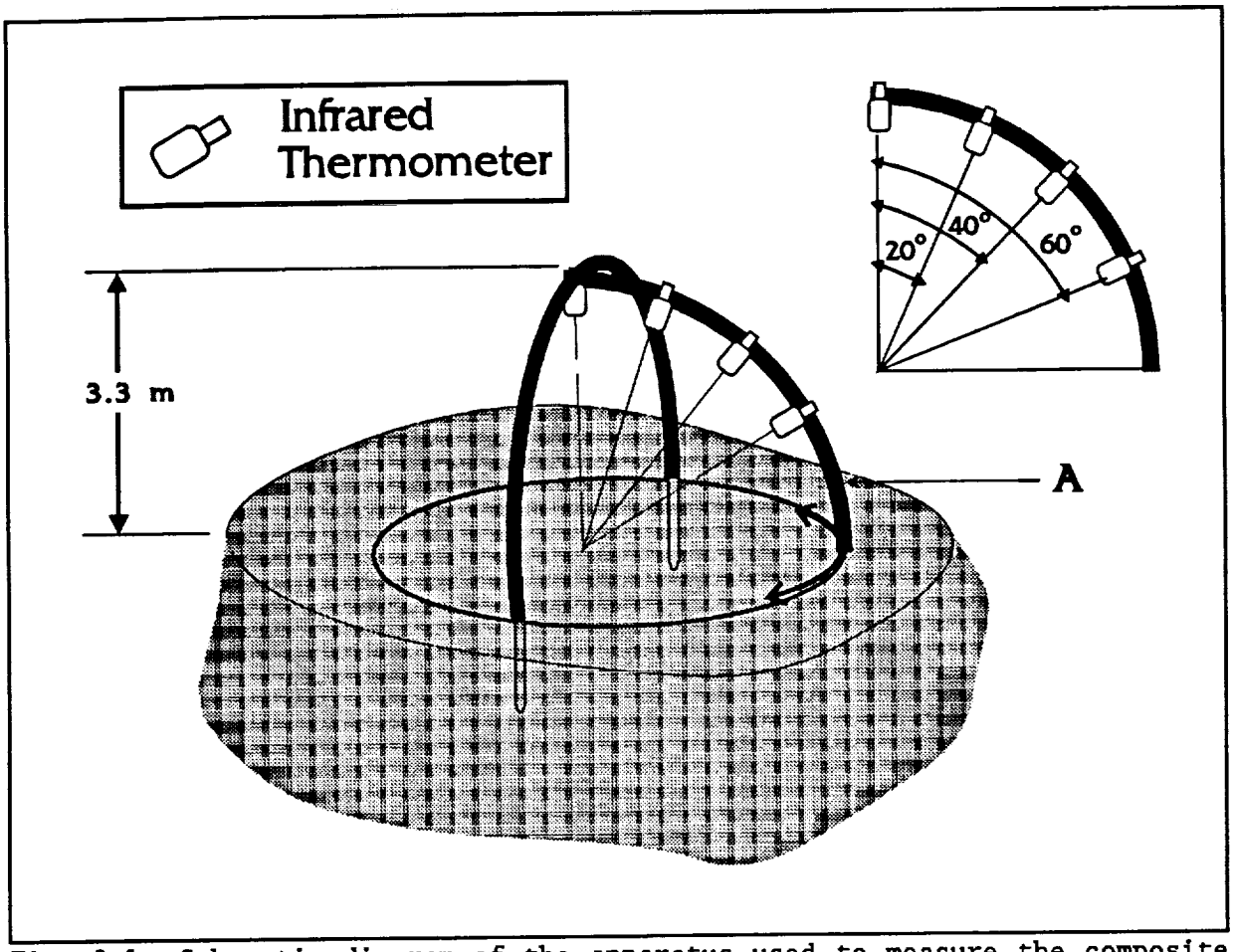

Fig. 3.1 Schematic diagram of the apparatus used to measure the composite temperatures. The arm (A) is free to revolve around the vertical axis.

where R_{bc} is radiative flux of the canopy measured with the IRT (i.e., $R_{bc} = \sigma T_r^4$); B* is background longwave (sky) radiation; ϵ_c is surface emissivity; and σ is the Stefan-Boltzmann constant. The surface emissivity was estimated using a modified pop-tent method described by Fuchs and Tanner (1966), and B* was estimated using the aluminum plate method described by Blad and Rosenberg (1976). IRT data were digitally recorded using Omnidata Polycorders, and later transferred to microcomputers for processing and analysis. Data were collected during periods when clouds did not obscure the Sun, which eliminated fluctuating surface temperatures caused by changing solar radiation flux densities.

H was estimated using the equation

$$H = \rho_a \, c_p \, (T_a - T_c) / r_a \,, \tag{3}$$

where ρ_a is the air density; c_p is the specific heat of air at constant pressure; T_a is air temperature; T_c is canopy temperature; and r_a is aerodynamic resistance to heat flow. We used the approach suggested by Hatfield et al. (1984) for estimating r_a:

$$r_a = [\ln (z - d) / z_o]^2 / (k^2 \, U) \,, \tag{4}$$

where z is height of meteorological observations; d is displacement height; z_o is roughness length; U is the horizontal wind speed; and k is von Karman's constant ($\approx$ 0.40). Roughness length is described as the point where the wind speed within the canopy reaches zero; displacement height is the mean level at which momentum is taken up by individual components of the canopy (Rosenberg et al., 1983). Using relationships given by Huband and Monteith (1986a, b) and Choudhury et al. (1986), d and z_o can be estimated from canopy height (h):

$$d = 2/3 \, h \tag{5}$$

$$z_o = h/8 \,. \tag{6}$$

Hatfield et al. (1984) suggested the use of Monteith's (1973) adjustment of r_a to correct for atmospheric stability. We found that better estimates of H were obtained if r_a values were not adjusted using this approach.

For comparison purposes, values of H were estimated with the eddy correlation and

the Bowen ratio techniques. For H calculated by the eddy correlation method (H_{ec}),

$$H_{ec} = \rho_a \, c_p \, \overline{w'\theta'} \tag{7}$$

where $\overline{w' \theta'}$ is the average of the product of the deviations from average of vertical wind velocity (w) and potential temperature (θ). For H calculated by the Bowen ratio method (H_{BR}),

$$H_{BR} = \rho_a \, c_p \, K_H \, (\delta T / \delta z) \tag{8}$$

where K_H is eddy diffusivity for heat; δT is temperature gradient; and δz is change in height. Half-hour averages of air temperature, air pressure, wind speed, and remotely-sensed canopy temperatures were used in (3)-(8) to estimate sensible heat flux.

3.3 Results and Discussion

Estimation of Sensible Heat Flux. In 1989, field measurements of canopy temperatures from different IRT view angles were taken on 5 days at two locations at the FIFE site. Hourly and daily averages of H were calculated with (3) using canopy temperatures, corresponding air temperatures and wind speeds from nearby automated weather stations. H was estimated with eddy correlation techniques on days 209 (July 28), 216 (August 3), and 220 (August 8), and with Bowen ratio techniques on days 218 (August 6) and 219 (August 7). Sensible heat fluxes calculated with the different approaches are given in Table 1.

TABLE 1. Values of Sensible Heat Flux Calculated by Hatfield et al. (1984) Method Using Canopy Temperature Data Obtained at Various IRT View Zenith Angles Compared to H Calculated by the Eddy Correlation (H_{cc}) or Bowen Ratio (H_{BR}) Methods.

Time LT	View Zenith Angle (degrees) 0	20	40	60	H_{cc} or H_{BR} (W m^{-2})
Day 209 (July 28)					
Daily Avg.	-140	-134	- 76	- 54	- 94
0800	- 35	- 27	- 60	- 58	- 36
0900	- 30	- 27	- 60	- 58	- 36
1000	-112	-108	- 62	- 53	- 86
1100	- 91	- 86	- 53	- 32	- 87
1200	-250	-236	-121	- 82	-125
Day 216 (August 3)					
Daily Avg.	19	- 13	56	59	- 72
1000	41	32	60	75	- 94
1300	- 30	- 56	5	4	- 76
1400	- 11	- 40	39	37	- 60
1500	79	21	122	126	- 66
1600	83	22	121	109	- 37
Day 218 (August 6)					
Daily Avg.	-144	-140	-106	- 49	-176
1000	-125	-117	-109	- 65	-158
1100	-141	-138	-112	- 68	-176
1200	-129	-130	-103	- 40	-202
1300	-150	-149	-149	-121	-184
1400	-187	-178	-116	- 51	-178
1500	-190	-181	-131	- 51	-161
1600	-100	-101	- 66	- 15	-138
Day 219 (August 7)					
Daily Avg.	-270	-265	-229	-104	-217
1100	-263	-251	-220	-102	-196
1200	-268	-256	-223	-103	-207
1300	-286	-289	-246	-110	-251
1400	-287	-287	-247	-123	-235
1500	-283	-271	-234	-109	-200
1600	-191	-182	-155	- 37	-153

Time LT	View Zenith Angle (degrees) 0	20	40	60	H_{ec} or H_{BR} (W m^{-2})
Day 220 (August 8)					
Daily Avg.	-230	-223	-192	-139	-116
1100	-156	-149	-126	- 90	-118
1500	-271	-262	-227	-165	-115
1600	-192	-187	-160	-117	-115

On days 209 and 219, days of moderate wind speeds (Table 2), H calculated using T_c measured at 40° agreed best with either H_{ec} or H_{BR} as compared to H estimated with T_c measured at the other view zenith angles. Estimates of H made with T_c data taken from any of the view zenith angles, except for 60° on day 219 and 0° and 20° at 1200 on day 209, agreed reasonably well with H_{ec} or H_{BR}.

TABLE 2. Average Wind Speeds for the Measurement Period of Each Day.

Day	Site	Time Interval LT	Wind Speed m s^{-1}
209	916	0815-1215	3.61
216	916	1115-1615	5.57
218	906	1015-1645	4.92
219	906	1145-1615	3.81
220	916	1215-1615	1.71

On day 220, a calm day, the best estimates of H were made using the 60° view zenith angle. Relatively poor agreement between H_{ec} and H estimated from the 0° and 20° T_c values was observed while H calculated with the 40° data tended to overestimate H compared to H_{ec}, but not so poorly as for the 0° and 20° data. On days of relatively high wind speed, that is, days 216 and 218, the best agreement between H calculated using T_c and H_{ec} or H_{BR} was obtained using the 0° and 20° data. In almost all cases there was a tendency

to underestimate the magnitude of the heat flux away from the canopies on these windy days. This was especially true on day 216. On that day, the eddy correlation calculation of H_{ec} always showed a sensible heat flux from the canopy to the air (negative sign), whereas H calculated with T_c data generally suggested heat flow to the canopy from the air. If r_a values used to calculate H from (3) were stability-corrected using the Monteith (1973) approach, the estimates of H on the windy days agreed slightly better with H_{ec} or H_{BR}. On days with moderate or especially low wind speeds, however, the stability correction produced estimates of H that agreed poorly with H_{ec} or H_{BR}.

It appears that the best view zenith angle to use for estimating H is dependent on wind speed. At wind speeds of less than about 4 m s^{-1}, good estimates of H can be made using surface temperatures made at the 40° view zenith angle, whereas for wind speeds greater than about 5 m s^{-1}, measurements of T_c at 0° or 20° work best.

The reason the view zenith angle changes with wind speed can be explained as follows. Mean tilt angle measurements suggested an erectophile type canopy (i.e., leaves that tend to be vertically oriented). The canopy did not completely cover the ground. Therefore, at the view angles of 0° and 20° and with the leaves in their normal position, the IRT would view the soil surface. The soil surface, especially at high solar elevations, would be warm relative to the vegetative cover, and the composite temperature of vegetative plus soil surfaces sensed by the IRT would be higher than the temperature of the vegetative surface. Therefore, using the temperature data taken at the 0° and 20° view zenith angle to calculate H would result in H rates that were too high. At the view zenith of 40° and 60°, the IRT would view mostly vegetation and would therefore sense a temperature more representative of the heat exchanging surface. At the 60° view zenith angle, the IRT would see a higher proportion of shaded leaves than at the 40° angle so the surface temperature would be

slightly cooler than the T_c representative of the heat exchanging surface and result in underestimation of H, as occurred on days 209 and 219.

With the higher wind speeds the canopy became more planophile, that is the leaves were more horizontally oriented, owing to the bending of the grass leaves. This reduced the amount of soil surface viewed by the IRT at the small zenith angles and, at the same time, it probably increased the amount of shadowed leaves seen by the IRT at the larger view zenith angles. As a result of this canopy distortion by the wind, the best angle to measure T_c for estimating H changed from 40° to a more vertically oriented angle.

3.4 Conclusions

Estimates of sensible heat flux made with remotely-sensed surface temperatures were calculated and compared to sensible heat flux values measured with micrometeorological techniques. Overall, the best estimates of H were made using canopy temperatures measured at the instrument view zenith angle of 40°. This finding is consistent with those of Zara (1992) who found that the average canopy temperature was obtained by making IRT measurements at a view zenith angle of about 40°. There was considerable variability, however, insofar as identifying the optimum view zenith angle with which to view the canopy at a specific time and under specific wind conditions.

Results suggested that the wind speed affected the optimum view zenith angle. Days with average wind speeds above 5 m s^{-1} coincided with the days on which the nadir and 20° view zenith angles provided canopy temperatures that resulted in the best estimates of sensible heat flux. On days with average wind speeds of less than 4 m s^{-1}, the 40° and 60° view zenith angles provided the best estimates of sensible heat flux. Wind speed should therefore be considered when selecting the appropriate view zenith angle for measuring canopy temperature to estimate sensible heat flux over prairie grasslands.

4. Extracting the Canopy Temperature from the Composite Temperature Measured by a Remote Sensor

4.1 Introduction

The use of remotely-sensed canopy temperature to infer soil and vegetation characteristics has been demonstrated in a number of studies. Canopy temperature can be used as an indicator of soil moisture status (Jackson, 1983) and plant water stress (Idso et al., 1977; Jackson et al., 1977a, 1977b) and hence, as a guide to irrigation scheduling (Jackson et al., 1977b; Gardner et al., 1981; Clawson and Blad, 1982) and as a means of assessing or predicting crop yields (Idso et al., 1977, 1979, 1980; Walker and Hatfield, 1979; Gardner et al., 1981; Smith et al., 1985).

With the advances in science and technology, it is now possible to measure the surface temperature on large spatial scale from airborne or spaceborne platforms. Studies to measure canopy temperature on a large spatial scale, however, have shown varying degrees of success (Heilman et al. 1976; Millard et al. 1978; Soer 1980; Price 1982; Cheevasuvit et al. 1985; Pierce and Congalton 1988). Success in measuring canopy temperature has been reported for surfaces with full vegetative cover but it has been difficult to estimate the canopy temperature when the cover is incomplete.

Much of this difficulty results because the temperature measured by a remote sensor is a composite temperature, i.e., the integrated temperature of the surfaces exposed to the instrument (e.g., canopy and its background). Previous studies have shown that the sensor view angle, canopy structure and percentage of ground coverage can affect the response of the thermal sensor (Hatfield, 1979; Kimes, 1980,1983; Kimes et al., 1980, 1981; Heilman et al., 1981; Parsons, 1985; Balick and Hutchinson, 1986; Paw U et al., 1989 among others). Depending on the percentage

of ground cover and viewing angle, the composite temperature can differ from the canopy temperature by as much as 13K (Kimes et al.,1980a; Hatfield, 1979).

Most managed and natural ecosystems are only partially vegetated during most part of the year. Therefore, to fully utilize the potential of thermal remote sensing technology in the management of our ecosystem, procedures to isolate the canopy temperature from the composite temperature are needed.

The problem of extracting the canopy temperature from the composite temperature has been investigated in many studies. Heilman et al. (1981) reported that the canopy temperature can be estimated from the composite temperature obtained from nadir view if percent ground cover, soil temperature, soil and canopy emissivities and sky irradiance are known. Other canopy temperature models with varying degree of complexity are also available (e.g., Sobrino and Caselles, 1990; McGuire et al. 1989; Choudhury and Idso, 1984; Kimes et al., 1981; 1980a; Welles et al., 1979; Jackson et al., 1979; Deardoff, 1978; Sutherland and Bartholic, 1977). However, the information required by these models may make them too complicated to implement on an operational basis.

The measurement of surface temperature by remote means is based on the principle of energy transfer by radiation, a process by which energy is transferred without the use of an intervening medium. According to the Stefan-Boltzmann law, the energy emitted is proportional to the fourth power of the absolute temperature of the body. For a blackbody (perfect absorber and radiator), the energy emitted (E) by a body (Wm^{-2}) is given as:

$$E = \sigma T^4 \qquad (4.1)$$

where T is the absolute temperature (K) and σ is a constant (5.67×10^{-8} $Wm^{-2}K^{-4}$).

Earth surface features are rarely, if ever, perfect absorbers or radiators thus, the energy measured by an instrument will include a reflected and emitted component. In this case the flux of radiation reaching a sensor (Es) is

$$Es = \epsilon\sigma T^4 + (1-\epsilon)B^* \quad (4.2)$$

where: ϵ is the emissivity and B* is the incoming longwave radiation (Fuchs and Tanner, 1966). Most thermal sensing instruments are fitted with filters that allow only the 8-14μm wavelength band to reach the sensor. In this radiation band, the emissivity of leaves and plant canopies is high. Idso et al. (1969) and Blad and Rosenberg (1976) reported emissivities of plant canopies greater than 0.97-0.98. Considering the high emissivity of plants and the factors involved in the measurement, Jackson (1983) suggested that for a surface temperature of 30°C, the error involved from assuming ϵ=1 would not generally exceed 1.0°C.

For first order approximation of actual surface temperature only direct line emission from the source to the sensor need be considered (Kimes et al., 1980a). The flux of radiation from a composite scene (e.g., canopy and background) to the sensor can then be approximated as:

$$T\Theta^4 = (1-f\Theta)Tc^4 + f\Theta Tb^4 \quad (4.3)$$

where: $T\Theta$ is the composite temperature (K) measured from view zenith angle Θ, Tc and Tb are the radiant temperatures of the canopy and background respectively (K); $f\Theta$ is the fraction of the background in the field of view of the instrument in the general direction of Θ or the so-called gap fraction or probability of gap (PGAPΘ).

Kimes et al. (1980a) tested the validity of Eq. (4.3) and reported close agreement between the theoretical and the observed values. To solve for Tc in Eq.

(4.3), TΘ, fΘ or PGAPΘ and Tb must be known. TΘ can be measured and PGAPΘ may be measured or estimated. The variable Tb is as difficult, if not more difficult to measure than Tc. To avoid the determination of Tb, Kimes (1981, 1983) suggested using multiple view angles. Use of multiple view angles, however is not economically feasible (Jackson et al. 1990).

Since the ultimate use of remotely-sensed temperature would probably come from aircraft of spacecraft, a procedure to isolate the temperature of the component of interest should be developed. The objective of this study was to develop a model simpler than the ones cited above which can be used on an operational basis to estimate the canopy temperature from the composite temperature as measured by a remote sensor.

4.2 Materials and Methods

The study was conducted at the University of Nebraska Agricultural Research and Development Center, Mead, Nebraska (41°9'N latitude and 96°30'W longitude) during the summer of 1990. Measurements were made over several plots of warm season range grasses seeded on Sharpsburg silty clay loam soil. The vegetation consisted of a mixture of big blue stem (Andropogon gerardii Vitnam), little bluestem (Schizachyrium scoparium (Michx.) Nash), indian grass (Sorghastrum nutans (L.) Nash), switch grass (Panicum virgatum L.) and sideoats grama (Bouteloua curtipendula (Michx.) Torr.).

During the experimental period, depending on the weather condition, as many plots as possible were selected to achieve a wide range of percent ground coverage. The plots had uniformly growing vegetation and an area of about $10m^2$. Some of the plots were located in areas that were under different grassland management practices

e.g., different cycles of burning or mowing, while others were in areas that were in their natural conditions. As such, background conditions differed from one plot to another, from one without debris to one covered with litter and dead plant material. Surface soil moisture conditions varied from moist to dry as estimated from visual observations. At the end of the experimental period, 14 plots were sampled in eight days during the period May to July.

Measurements. Composite temperatures (TΘ) were measured with four Everest 4000 Multiplexer-Transducer (Everest Interscience, Inc.) while canopy temperature (Tc) and background temperature (Tb) were measured with a handheld infrared thermometer (Scheduler Plant Stress Monitor, Ohio Standard Oil). The infrared thermometers (IRT) have 15° field of view (FOV), bandpass of 8-14 μm, accuracy of 0.5K and resolution of 0.1K.

The four transducers were mounted on an arc at angles of 0°, 20°, 40° and 60° from the vertical (Fig. 3.1). The arc was made such that the field of view of each instrument was centered on the same point on the ground at a distance of 3.3 meters. It was supported on one end by a semi-circular arc and was free to revolve around the vertical axis. The height of the arc was adjusted to maintain a distance of 3.3m above the average height of the vegetation.

During the measurement periods the arc was centered over the plot. Composite temperature readings were taken with the arc aligned towards each of the eight cardinal compass directions. Immediately after the composite temperature readings were taken, canopy and background temperatures were measured with a handheld IRT. Canopy temperature was measured by placing the handheld IRT very close to the canopy in an almost horizontal position. Mean canopy temperature was

obtained by taking the average of eight readings taken from the eight major compass directions. Mean background temperature was obtained by taking the average of several readings taken from different points on the ground with no foliage in the instrument field of view. Air temperature was also monitored by another sensor in the Scheduler. All measurements were replicated twice.

Field checking of the instruments was done by comparing the IRT readings to a blackbody calibration source (Everest 1000, Everest Interscience, Inc.) before and after each set of readings. The IRTs were also calibrated in the laboratory before and after the experimental period. There were no significant changes observed in the calibrations.

Measurements were made on clear days or during periods when no clouds obscured the sun. It took about five minutes to finish each set of readings. All measurements were made during mid-day, 1200-1500h. This time is considered optimum for many remotely-sensed temperature applications (Gardner et al. 1981; Millard et al., 1978).

Plant parameters measured were leaf area index (LAI) and gap fractions (PGAPΘ) and canopy heights. LAI and PGAPΘ were measured using the LiCor Plant Canopy Analyzer (LAI 2000, LiCor Inc., Lincoln, NE). This instrument consists of an optical sensor and a control unit. The sensor is made of five concentric rings of radiation detectors. The lenses in front of the detectors cause the five rings to see different portions of the sky. The sensor has a filter that rejects light greater than 0.490 μm, thus minimizing the light reflected and transmitted by leaves from reaching the detectors. The control unit records light readings above and below the canopy at five angles and calculates LAI and PGAPΘ from light interception measurements.

4.3 Results and Discussions

Data gathered throughout the experiment are presented in Tables 4.1, 4.2 and 4.3. Table 4.1 presents the grassland management practices (Treatments), percent ground cover (GC), LAI and canopy height. Table 4.2 presents the gap fractions (PGAPΘ) from the four view zenith angles. Leaf Area Index (LAI) ranged from 0.66 to 3.81 while gap fractions at nadir ranged from 0.17 to 0.86. Canopy height ranged from 0.15 to 0.65m. Table 4.3 presents the temperature measurements made on each plot. The measurements were made on different days with different environmental conditions and air temperatures ranging from 297 to 315K during the time of measurement. Canopy temperatures ranged from 295 to 314K while background temperatures ranged from 307 to 332K.

Table 4.1. Management practices (Treatment), percent ground cover (GC), Leaf Area Index (LAI) and plant height.

PLOT	Treatment[1]	GC (%)	LAI	HEIGHT (m)
1	a	14	0.66	0.15
2	a	25	1.35	0.20
3	b	37	1.58	0.25
4	c	45	2.08	0.45
5	d	67	2.66	0.55
6	b	60	2.76	0.60
11	e	27	1.42	0.25
12	e	41	1.65	0.35
13	f	85	3.81	0.65
14	c	52	2.15	0.60
15	g	35	1.56	0.25
16	b	57	2.36	0.50
17	b	43	1.75	0.40
18	h	70	2.79	0.60

[1] a- Burned in Fall of 1989
b- Mowed in Fall of 1989 and litter left behind
c- Control, natural condition
d- Mowed in Summer of 1989 and litter left behind
e- Burned in Summer of 1989
f- Burned in May 1990
g- Mowed in Fall of 1989 and litter removed
h- Mowed in Summer of 1987 and litter removed

Table 4.2 GAP Fractions (PGAPΘ) measured from 0°, 20°, 40° and 60° view zenith angles.

PLOT	PGAP0	PGAP20	PGAP40	PGAP60
1	0.856	0.781	0.713	0.385
2	0.745	0.669	0.521	0.314
3	0.630	0.486	0.339	0.216
4	0.550	0.395	0.238	0.134
5	0.432	0.286	0.158	0.080
6	0.400	0.254	0.153	0.094
11	0.748	0.690	0.422	0.269
12	0.591	0.463	0.343	0.219
13	0.174	0.095	0.055	0.031
14	0.479	0.327	0.232	0.121
15	0.648	0.526	0.386	0.244
16	0.429	0.322	0.217	0.113
17	0.573	0.432	0.259	0.157
18	0.300	0.222	0.147	0.069

From the 14 plots, five (2, 4, 13, 15 and 16) were selected for use in the subsequent discussion and model development. These plots represented the range of ground covers (i.e., (1-PGAP at nadir)x100) that were observed in the field, from very sparse (25% ground cover) represented by Plot 2 to almost full cover (86% ground cover) represented by Plot 13. Plots 4, 15 and 16 have intermediate ground cover, 45, 35 and 57% respectively (see Table 4.1). Soil surfaces of plots 2 and 4 were relatively moist while plots 13, 15 and 16 were relatively dry. Weather conditions during the time of measurement varied from relatively cool with air temperatures of 297.9 and 307.5K for plots 2 and 4, respectively to relatively warm

Table 4.3 Composite temperatures (TΘ) measured from 0°, 20°, 40° and 60° view zenith angles, canopy temperature (Tc), background temperature (Tb), and air temperature (Ta). All units are in K. Measurements were made on eight days during the period May-July.

PLOT	T0	T20	T40	T60	Tc	Tb	Ta
1	307.96	306.70	302.40	300.82	295.50	311.83	297.61
2	308.31	306.96	303.28	299.61	295.62	309.51	297.91
3	310.65	308.69	306.31	302.29	299.84	312.27	304.28
4	308.98	307.88	305.61	302.45	300.93	312.47	307.52
5	310.79	310.53	307.68	305.94	304.80	314.66	307.43
6	304.35	304.09	301.21	300.56	299.70	307.16	303.59
11	326.27	325.27	321.46	317.02	313.80	332.80	314.30
12	322.18	320.27	317.00	313.77	311.40	329.20	314.75
13	309.00	308.89	308.45	307.92	307.40	312.50	313.85
14	319.74	318.59	315.65	313.10	311.70	324.65	314.35
15	320.98	319.52	316.81	312.35	309.65	326.65	313.85
16	318.82	317.42	314.73	312.30	311.25	324.20	315.70
17	320.36	318.68	316.15	312.70	310.85	326.55	314.50
18	313.90	313.29	311.06	310.37	309.50	315.20	314.55

with air temperatures greater than 313K for plots 13, 15 and 16 (see Table 4.3). Data from the remaining nine plots served to validate the model.

Variation of Composite Temperature with View Angle. Figure 4.1 shows a graph of composite temperature (TΘ) as a function of view zenith angle for the five selected plots. Since the data were gathered on different days with different environmental conditions, there are differences in TΘ. For example, Plots 2 and 13 were measured on two different days with an air temperature difference of about 16K but their composite temperatures at nadir differed by less than 1K. On the other hand, Plots 15 and 16 were measured on the same day with approximately the same air temperature but their composite temperature at nadir differed by about 10K. In general, for measurements made under similar weather conditions, TΘ increased

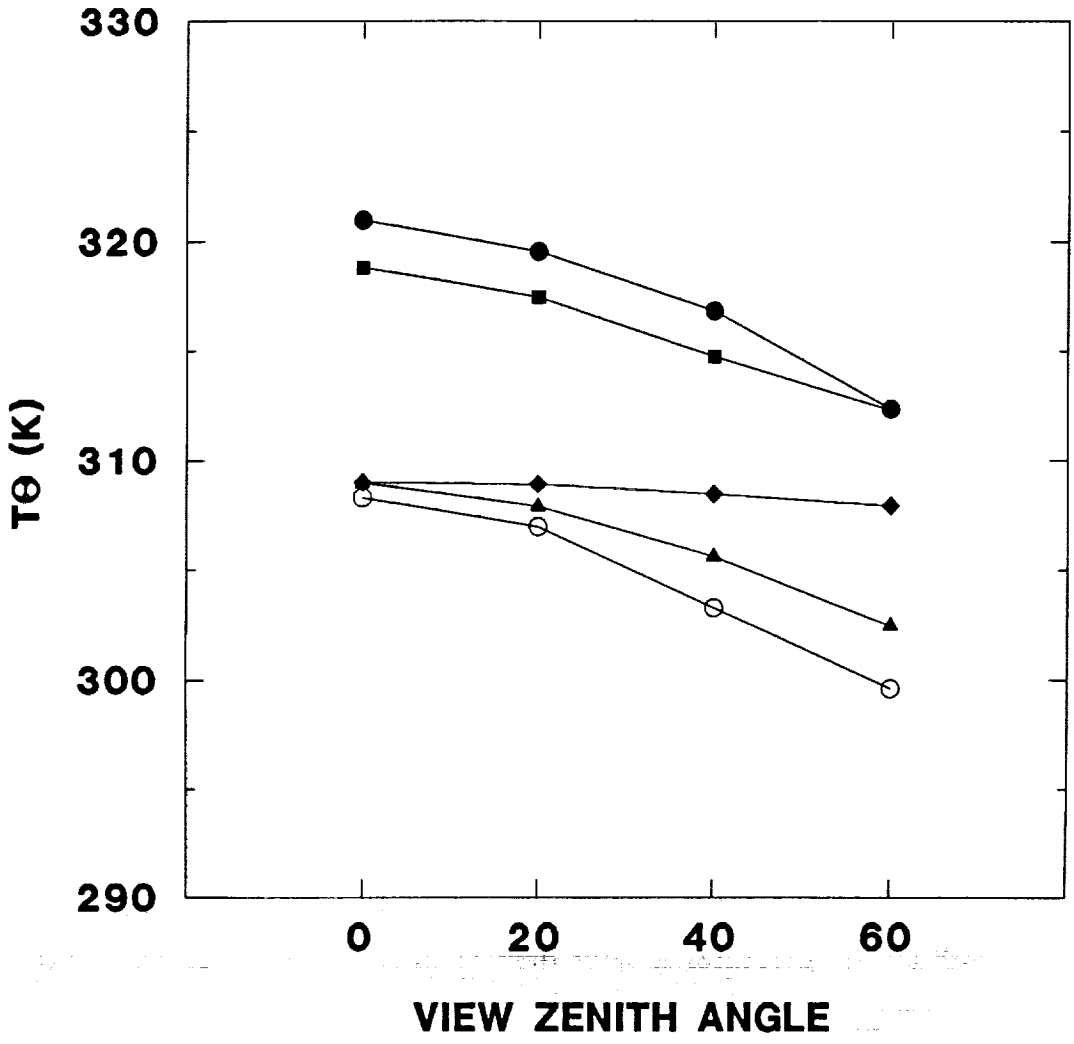

Figure 4.1. Composite temperatures (TΘ) as a function of view zenith angle for the different plots (○)P2, (●)P15, (▲)P4, (■)P16 and (♦)P13.

with a decrease ground cover or LAI. At low percentage of ground cover, absorption of solar radiation by soil and canopy is enhanced (less shading) resulting in a higher soil and canopy temperature compared to plots with higher percentage of ground cover. The high proportion of warm soil in the field of view of the instrument in addition to the warm canopy results in a higher composite temperature.

For a particular plot, TΘ decreases with increasing view angle. This trend is expected because at increasing view angle the proportion of the background in the field of view of the instrument is decreased while that of the canopy is increased. Since the background was at a higher temperature than the canopy (Table 4.3) the resulting composite temperature was lower. There are also differences in the magnitude of changes of TΘ from one plot to another. The variation of TΘ with view angle decreases with increasing ground cover. Plot 2, which had the sparsest canopy, showed the greatest variation of TΘ with view angle. For this plot TΘ decreased by about 8K from nadir to the 60° view angle. Plot 13, which was almost at full cover, showed very little variation (about 1K) with view zenith angle.

The variation of TΘ with view angle from plot to plot can be explained by the magnitude of the change in the proportion of the canopy and background in each view angle (Fig. 4.2). At low ground cover (e.g., Plot 2) the change in the proportion of gap with view angle was higher as indicated by the steeper slope of the line. At increasing ground cover the rate of change becomes less as indicated by the decreasing slope of the lines.

Deviation of Sensor Response from the Canopy Temperature. Information concerning the magnitude of the deviation of TΘ from Tc that might be expected from a given ground cover condition is important if one is to infer canopy temperature from composite temperature measurements. Deviations of TΘ from Tc, i.e., (TΘ-Tc) as a function of view angle for the five selected plots are shown in Fig. 4.3. For the sparsest canopy (Plot 2), TΘ differed from Tc by about 5K when viewed at 60° and more than 13K when viewed at nadir. For canopies with nearly

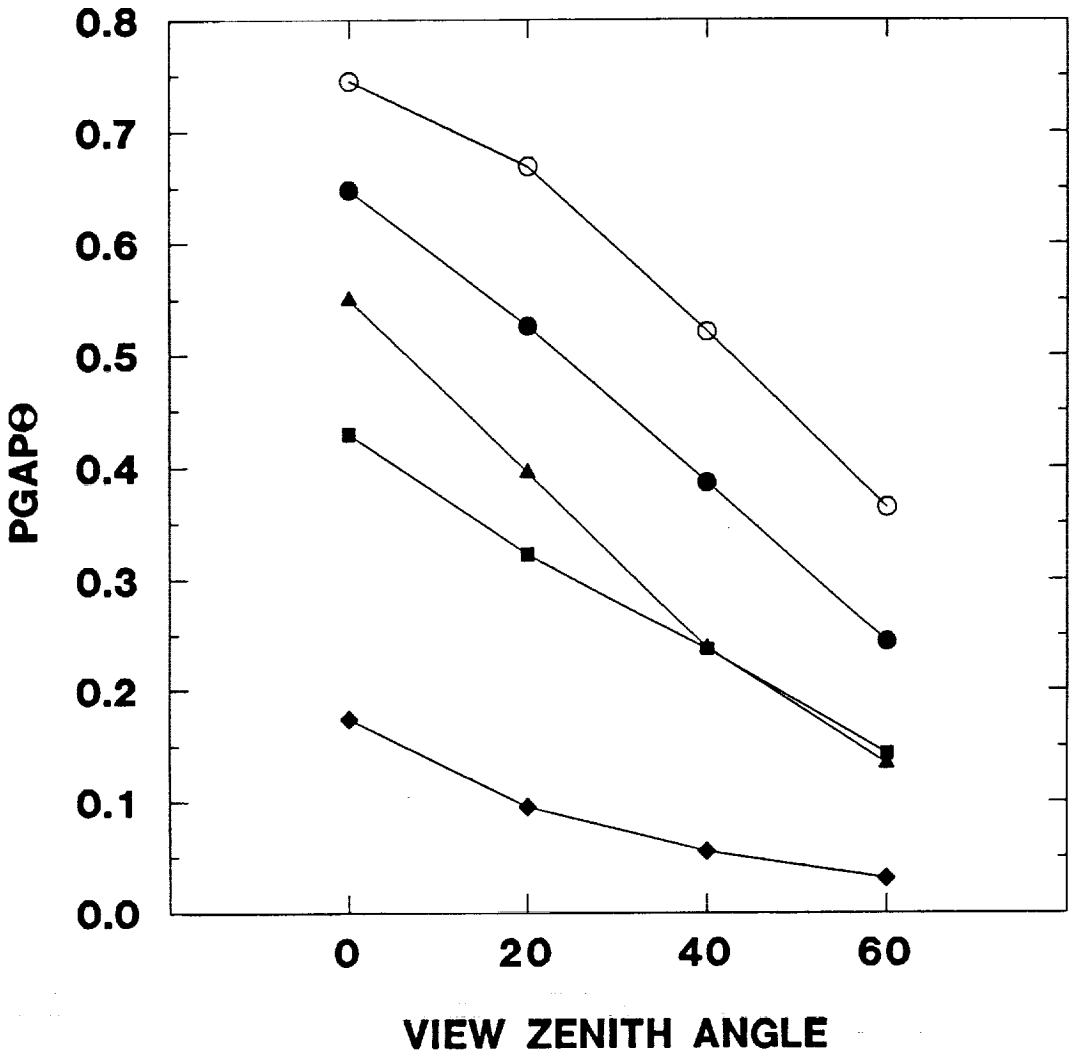

Figure 4.2. Gap distribution (PGAPΘ) as a function of view zenith angle for plot (○)P2, (●)P15, (▲)P4, (■)P16) and (♦)P13.

complete cover (Plot 13) there was very little variation with view angle. For a particular view zenith angle, (TΘ-Tc) decreased with increasing LAI or ground cover.

Differences in the magnitude of deviations (TΘ-Tc) from one plot to another were due to differences in PGAPΘ and (Tb-Tc). This can be readily explained by rewriting Eq. (4.3) so that

$$T\Theta^4 - Tc^4 = PGAP\Theta(Tb^4 - Tc^4) \qquad (4.4)$$

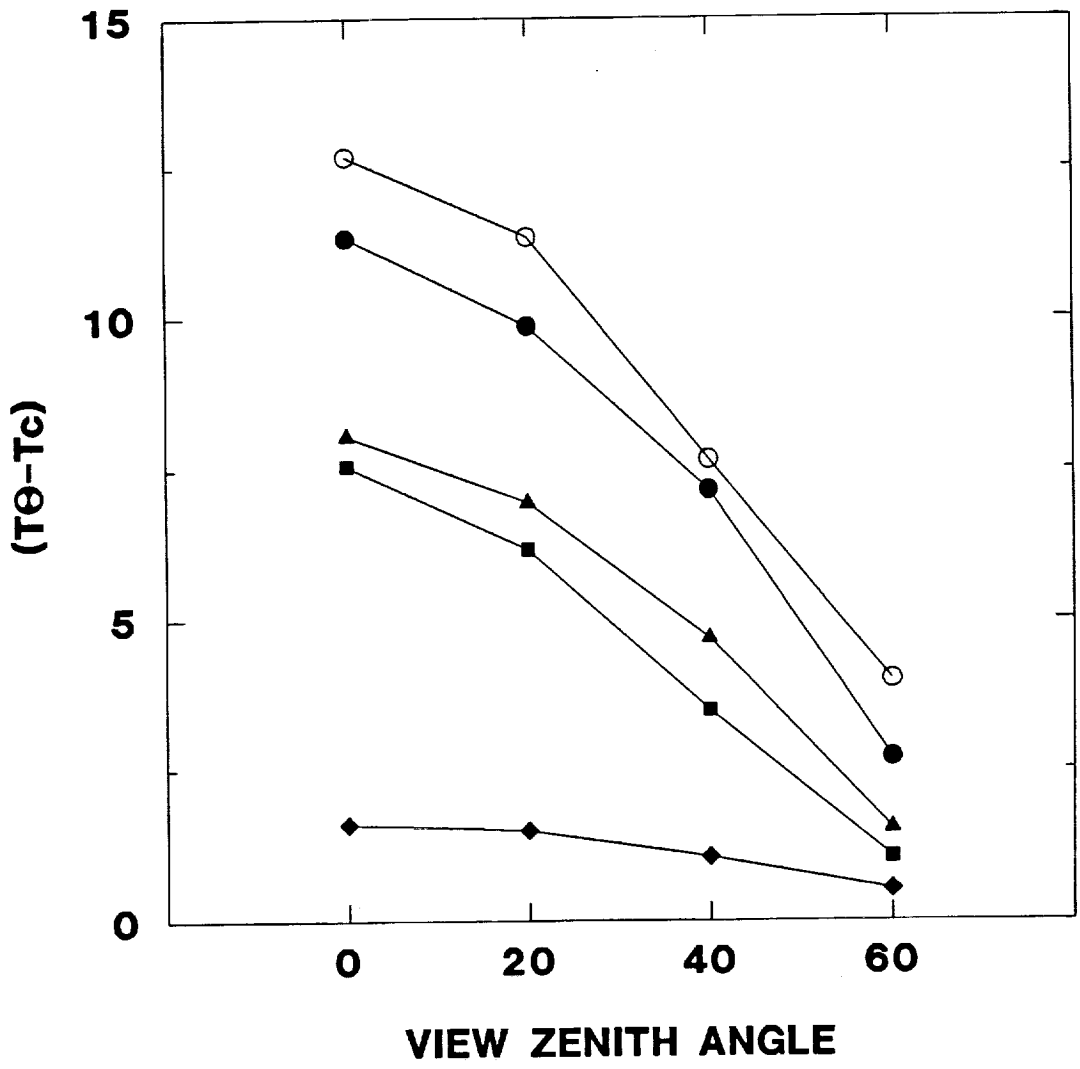

Figure 4.3. Deviation of the composite temperature from the canopy temperature (TΘ-Tc) as a function of view zenith angle for plot (○)P2, (●)P15, (▲)P4, (■)P16 and (◆)P13.

Equation (4.4) suggests that the deviation of TΘ from Tc will be greatest when PGAPΘ and/or (Tb^4-Tc^4) are high. PGAPΘ and (Tb-Tc) are directly related to each other, i.e., when PGAPΘ is high, (Tb-Tc) is also high. This phenomenon is so because at high PGAPΘ the differential heating between the ground and canopy is enhanced, creating a wide difference between the ground and canopy temperature.

At low PGAPΘ, less solar radiation reaches the soil and the differential heating is suppressed (Kimes et al.,1980).

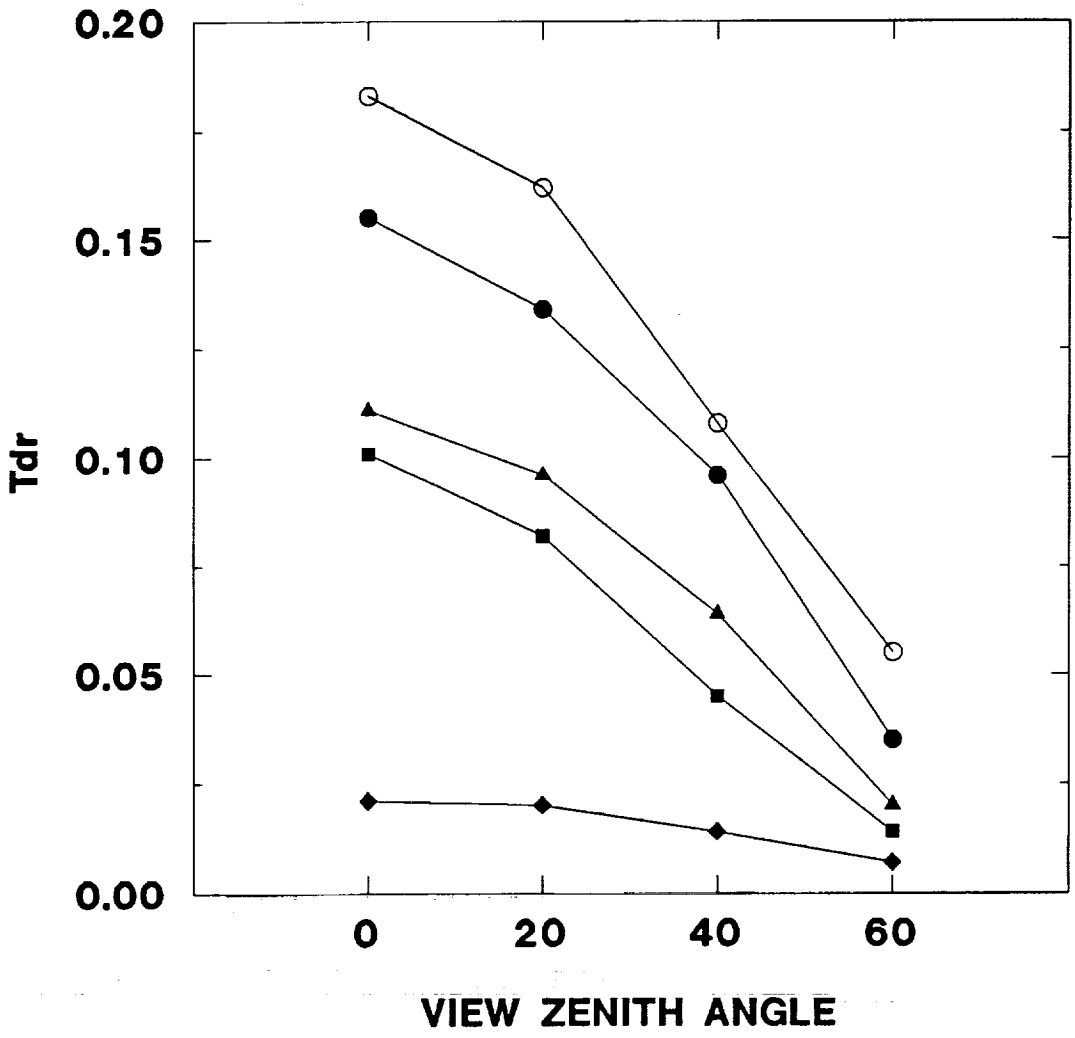

Figure 4.4. Deviation of the composite temperature relative to the canopy temperature (Tdr) as a function of view zenith angle for plots (○)P2, (●)P15, (▲)P4, (■)P16 and (◆)P13.

Figure 4.3 gives an indication of the absolute deviations for the range of conditions in which the data were gathered. However, for another set of environmental conditions the above deviations may be quite different. Transforming the deviations into values relative to the canopy temperature (i.e.,

$Tdr=(T\Theta^4-Tc^4)/Tc^4)$ will give Fig. 4.3 a wider range of applicability. The relationship of Tdr to view angle is shown in Fig. 4.4. Although Figs. 4.3 and 4.4 look similar, the information derived from the two figures is different. Figure 4.3 gives deviations that are absolute while Fig. 4.4 gives relative deviations that change with environmental conditions.

Modeling the Canopy Temperature. To be able to use Eq. (4.3) in operational situations, simplifying procedures and assumptions need to be made. Equation (4.3) can be rewritten as:

$$Tdr = PGAP\Theta((Tb^4/Tc^4)-1) \tag{4.5}$$

where:

$$Tdr = (T\Theta^4 - Tc^4)/Tc^4 \tag{4.6}$$

The variables on the right hand side of Eq. (4.5) are directly related to each other. The ratio, Tb^4/Tc^4 increases with increasing PGAP (Fig. 4.5). For a given plot Tb^4/Tc^4 is constant during the angular measurement period. At another weather condition, Tb^4/Tc^4 may be assumed to be relatively constant. Due to the nature of the heating process and to differences in heat capacities between the soil and vegetation it is very likely that a change in Tb will have a proportionate change in Tc. This phenomenon can be substantiated by the data from Kimes et al. (1980a) which indicated that for a particular plot Tb/Tc stayed relatively constant for the dawn measurements and those made near noon. With this, it follows that at other weather condition Tb/Tc can be assumed to be relatively constant. Thus, Tb^4/Tc^4 can be dropped from Eq. (4.5) and replaced by a constant (C), i.e.,

$$Tdr = CPGAP\Theta \tag{4.7}$$

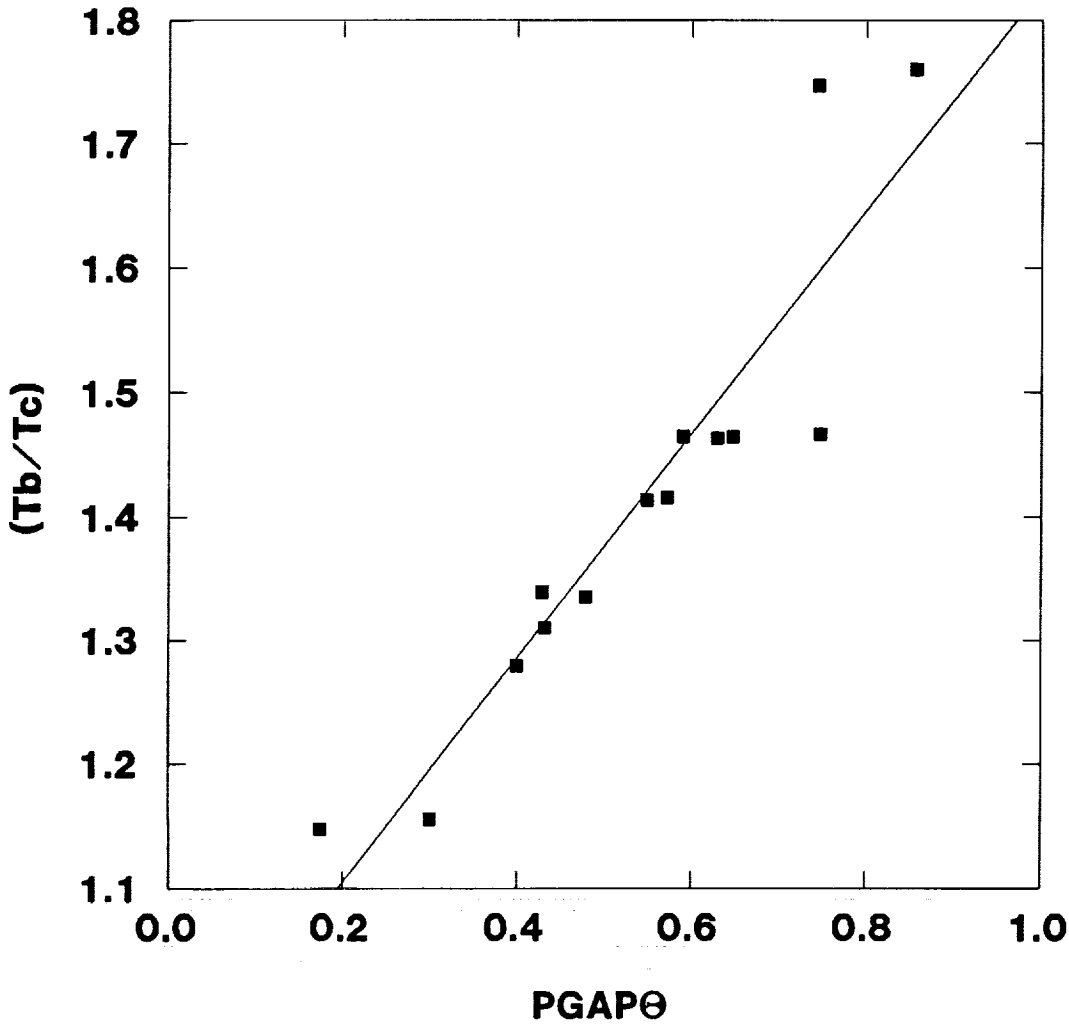

Figure 4.5. Relationship of the ratio of Tb/Tc to PGAPΘ for the five selected plots.

The constant (C) can be evaluated by regression techniques. Once C is known, Tc can be calculated from Eq. (4.6).

Tdr values for each zenith view angle were calculated for the five plots and plotted against PGAPΘ (Fig. 4.6). As expected from Eq. (4.7), a direct linear relationship existed between Tdr and PGAPΘ (r^2=0.97). Using a linear regression technique, C was found to be 0.231.

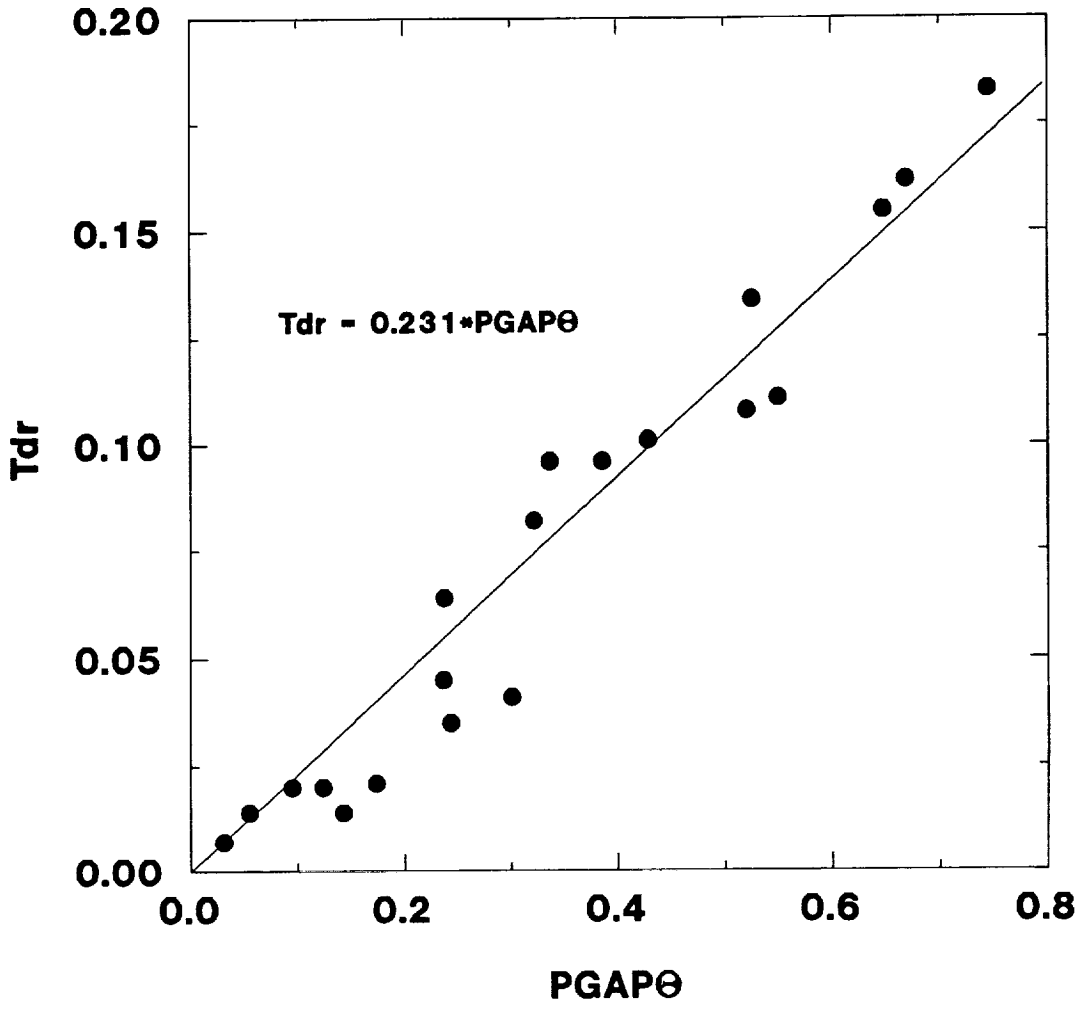

Figure 4.6. Relationship of relative temperature difference (Tdr) to PGAPΘ. The solid line is the equation Tdr = 0.231PGAPΘ.

Combining Eqs. (4.6) and (4.7) and solving for Tc yields:

$$Tc = T\Theta(1.0+0.231PGAP\Theta)^{-0.25} \qquad (4.8)$$

The variables on the right hand side of Eq. (4.8) may be obtained by remote means as will be shown in Sec. 6. Thus the canopy temperature, Tc can be estimated from Eq. (4.8) using only remotely-sensed information.

Leaf Area Index (LAI) may also be used in Eq. (4.6) instead of PGAPΘ. The two variables are related to each other by the following equation:

$$PGAP\Theta = \exp(-kLAI/\cos\Theta) \quad (4.9)$$

where LAI is the leaf area index; Θ is the zenith view angle; and k is the proportion of the canopy projected in the general direction of Θ. Using Eq. (4.9) in place of $PGAP\Theta$, however, makes the model crop specific because the variable k depends on the geometric structure of the crop.

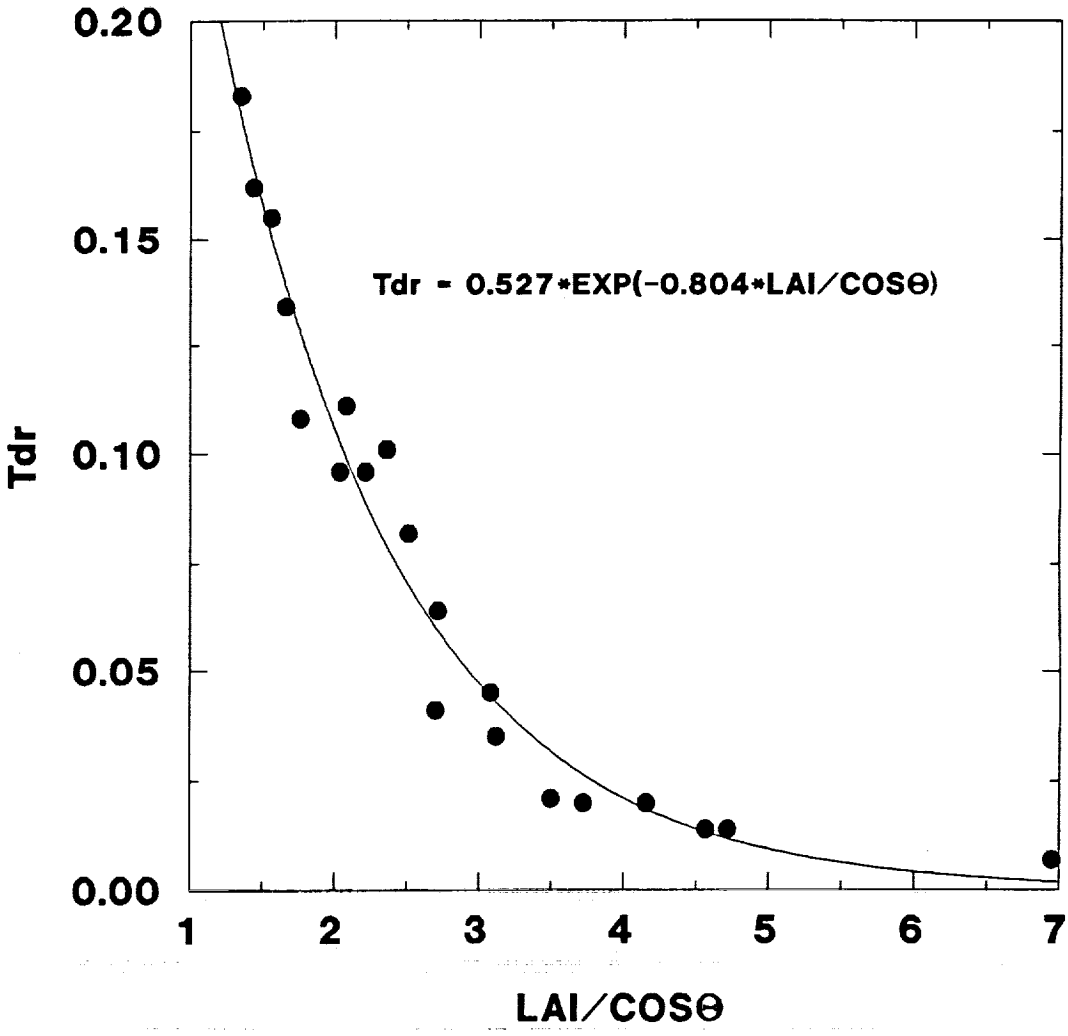

Figure 4.7. Relationship of relative temperature difference (Tdr) to LAI/cosΘ. The solid line is equation Tdr = 0.527exp(-0.804LAI/cosΘ).

A plot of Tdr as a function of LAI/cosΘ is shown in Fig. 4.7. The equation which fits the data (r^2=0.98) is

$$Tdr = 0.527\exp(-0.804LAI/\cos\Theta) \quad (4.10)$$

Substituting Eq. (4.10) into Eq. (4.6) and solving for Tc yields:

$$Tc = T\Theta(1.0+0.527\exp(-0.804LAI/\cos\Theta)^{-0.25} \quad (4.11)$$

LAI can be estimated from remotely-sensed data as has been demonstrated in a number of studies (e.g., Asrar et al., 1985; Hatfield et al., 1984; Gardner et al., 1986). Thus, Eq. (4.11) can be used to estimate Tc by remote means.

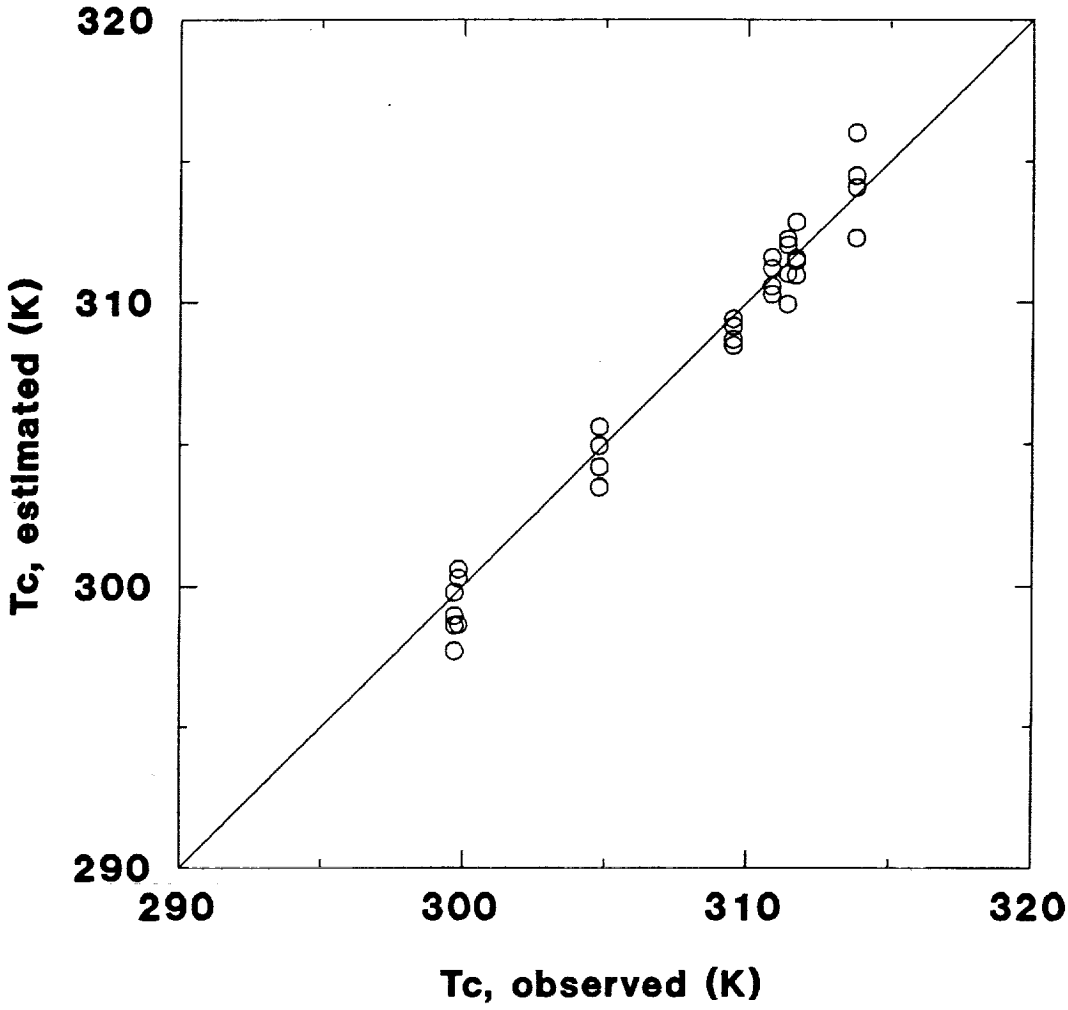

Figure 4.8. Comparison of canopy temperature estimated from $Tc = T\Theta(1.0+0.231PGAP\Theta)^{-0.25}$ with the observed values. The solid line is the 1:1 line.

Model Validation/Testing. Equations (4.8) and (4.11) were applied to the rest of the data gathered in this experiment. Comparisons of the estimated canopy temperatures with the measured values are shown Figs. 4.8 and 4.9. Good agreement was obtained between the estimated and observed Tc values with the d index (Willmott, 1982) of 0.99 for both equations and RMSE=0.54 and 0.56 for Eq. 4.8 and 4.9, respectively.

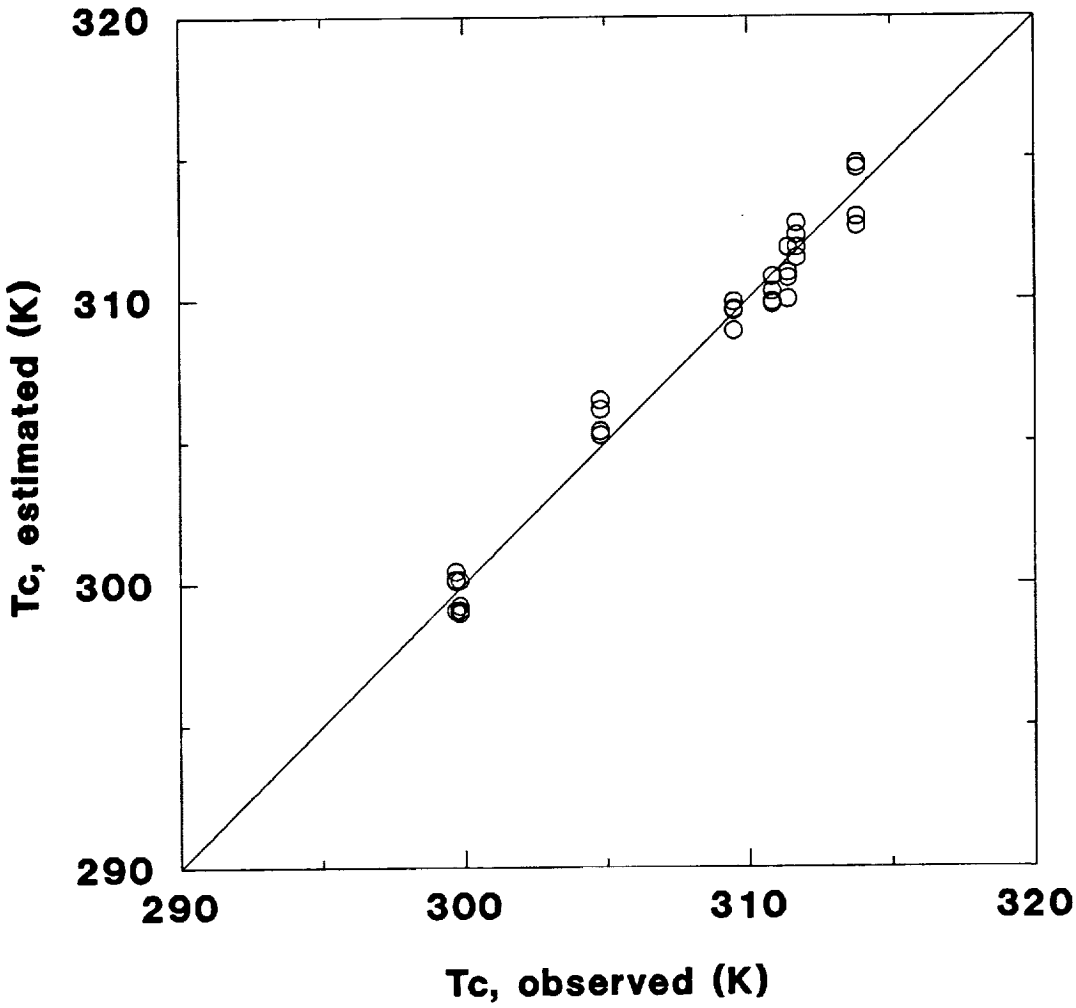

Figure 4.9. Comparison of canopy temperature estimated from $Tc = T\Theta(1.0+0.527\exp(-0.804LAI/\cos\Theta)^{-0.25}$ with the observed values. The solid line is the 1:1 line.

Equation 4.8 was further tested using the data from Matthias et al. (1987). Their data were obtained from cotton (Gossypium hirsutum L. Deltapine 61) grown in a portable wooden box (0.5 X 0.5 X 0.28m) containing Vinton loamy fine sand. The plants were 0.15m tall and had six leaves/plant with a total area of 0.025m². The data set consists of composite temperatures obtained from nadir view, canopy temperatures and gap fractions. Composite temperatures were varied by viewing different proportions of canopy and background at nadir. This was done by moving

the box across the stationary field of view of the instrument. Results of the validation is shown in Table 4.4. Good agreement was obtained between the modeled and measured canopy temperatures with a RMSE of 0.53.

Table 4.4. Composite temperature (T0), Gap fraction (PGAP), measured canopy temperature (Tc), modeled canopy temperature (Tcmod) estimated from equation (4.8) and difference between the measured and modeled canopy temperature (Tc-Tcmod). Experimental data were obtained from Matthias et al., (1987).

T0 °C	PGAP °C	Tc °C	Tcmod °C	Tc-Tcmod °C
33.20	0.78	21.2	20.87	0.33
30.80	0.63	21.2	20.65	0.55
27.20	0.34	21.2	21.57	-0.37
25.50	0.31	21.2	20.45	0.75

4.4 Summary and Conclusions

Sec. 4. documents the angular variation of composite temperature measured by a remote sensor for grassland vegetation. Depending on the percentage of ground cover and zenith view angle from which the measurement was made, the composite temperature may differ from the canopy temperature by as much as 13K. The deviations were found to be linearly related to the gap distribution in the canopy and exponentially related to LAI/cosΘ. Two models, Eq. (4.8) and Eq. (4.11), were developed to estimate the canopy temperature using primarily remotely-sensed information. Good agreement was found between the model estimates and measured canopy temperature with RMSE of 0.54 and 0.56 for Eq. (4.8) and Eq. (4.11), respectively. Application of the model to limited data from the literature indicated

good agreement between the estimated and the measured canopy temperature (RMSE = 0.53).

Although the models were developed from data acquired from plots with a wide range of ground cover and environmental conditions, further studies are needed to assess the stability of the empirical but physically based coefficients. The models presented here were developed for grass covered surfaces but a similar procedure may be used to develop models for agricultural crops and other natural ecosystems (e.g., forest).

5. Modeling the Mean Composite Temperature of Partially Vegetated Surfaces

5.1 Introduction

Remotely-sensed surface temperature can be used to help estimate sensible heat flux (H) and latent heat flux (LE) over large areas. In an approach described by Jackson (1985), H is estimated using the bulk transfer equation given as:

$$H = \rho Cp(Ts-Ta)/ra \qquad (5.1)$$

where ρ is the density of the air (kg m^{-3}), Cp specific heat of the air (J $kg^{-1}K^{-1}$), Ts and Ta are the surface and air temperature (K), respectively, and ra is the aerodynamic resistance to heat transfer (sm^{-1}). LE is estimated as the residual in the energy budget equation given as:

$$-LE = R_n + H + S \qquad (5.2)$$

where R_n is the net radiation and S is the soil heat flux. Using this approach, satisfactory estimates have been reported for surfaces with essentially full vegetative cover (Hatfield et al., 1983; Seguin and Itier, 1983; Reginato et al.,1985; Moran et al.,1989), but difficulties arise when a surface is only partially covered with vegetation (Kustas et al., 1987).

Most of the work done to overcome the difficulties in estimating H has focused on adjusting the resistance to heat transfer (Kustas et al., 1989; 1990). This adjustment however, does not seem to be applicable in all circumstances as suggested by their recent findings where the modeled sensible heat flux disagreed with the measured flux not only in magnitude but also in sign. Hence, factors other than the aerodynamic resistance may need to be considered.

The reliable evaluation of sensible heat flux using Eq. (5.1) by remote means is based on the assumption that the temperature measured by a remote sensor (Ts)

is the aerodynamic temperature, i. e., the average temperature of all the canopy elements weighted by the relative contribution of each element to the overall aerodynamic conductance (McNaughton, 1988; Moran et al., 1989). Due to directional characteristics of radiometric temperature, Huband and Monteith (1986) stated that the radiometric (i.e., temperature obtained by a radiometer) and aerodynamic temperature may not be the same for a crop canopy. Choudhury et al. (1986) found that the two are nearly the same for near neutral conditions, but radiometric temperatures were higher than the aerodynamic temperatures for stable conditions and lower for unstable conditions.

The disagreement between radiometric and aerodynamic temperature is further complicated when the surface is only partially vegetated. In this case, the temperature measured by a remote sensor is the integrated temperature of the surfaces exposed to the instrument. Currently, for most large area application studies, the surface temperature is measured at nadir view. At this view angle the temperature measured may be dominated by the temperature of the soil surface which is usually higher than the temperature of transpiring vegetation during the day. Thus, for partially vegetated surfaces H is commonly overestimated and LE is underestimated (Moran et al., 1989). Clearly, the temperature measured at nadir will not likely represent the temperature of the heat exchanging surface.

The dependence of remotely-sensed surface temperature on viewing angles and directions has been reported in a number of studies (e.g. Fuchs et al., 1967; Kimes et al., 1980, 1981; Heilman et al., 1981; Parsons, 1985). However, the question of which directional temperature measurement best represents the surface temperature of partially vegetated surfaces for use in radiation or energy balance

studies has not been fully addressed. Procedures for obtaining the representative surface temperature to use for a given application and degree of ground cover are lacking. The objective of this study is to develop a procedure for obtaining/estimating the mean composite temperature of partially vegetated surfaces from directional radiometric measurements.

5.2 Materials and Methods

The study was conducted at the University of Nebraska Agricultural Research and Development Center, Mead, Nebraska (41°9'N latitude and 96°30'W longitude) during the summer 1990. Measurements were made over several plots of warm season range grasses seeded on Sharpsburg clay loam soil. The vegetation consisted of a mixture of big blue stem (*Andropogon gerardii* Vitnam), little bluestem (*Schizachyrium scoparium* (Michx.) Nash), indian grass (Sorghastrum nutans (L.) Nash), switch grass (*Panicum virgatum* L.) and sideoats grama (*Bouteloua curtipendula* (Michx.) Torr.).

During the experimental period, depending on the weather condition, measurements were obtained on as many plots as possible to achieve a wide range of percent ground coverage. Each plot had uniformly growing vegetation and an area of about $10m^2$. Some of the plots were located in areas that were under different grassland management practices e.g., different cycles of burning or mowing, while others were in areas that were in their natural conditions. As such, background conditions differed from one plot to another, from one without debris to one covered with litter and dead plant material. Surface soil moisture conditions varied from moist to dry as estimated from visual observations. At the end of the experimental period, 14 plots were sampled in eight days during the period May to July.

Measurements. Composite temperatures ($T\Theta$) were measured with four Everest 4000 Multiplexer-Transducer (Everest Interscience, Inc.) while canopy temperature (Tc) and background temperature (Tb) were measured with a handheld infrared thermometer (Scheduler Plant Stress Monitor, Ohio Standard Oil). The infrared thermometers (IRT) have 15° field of view (FOV), bandpass of 8-14 μm, accuracy of 0.5K and resolution of 0.1K.

The transducers were mounted on an arc at angles of 0°, 20°, 40° and 60° from the vertical. The arc was made such that the field of view of each instrument was centered on the same point on the ground at a distance of 3.3 meters. It was supported on one end by a semi-circular arc and was free to revolve around the vertical axis. The height of the arc was adjusted to maintain a distance of 3.3m above the average height of the vegetation.

During the measurement periods the arc was centered over the plot. Composite temperature readings were taken with the arc aligned towards each of the eight cardinal compass directions. Immediately after the composite temperature readings were taken, canopy and background temperatures were measured with a handheld IRT. Canopy temperature was measured by placing the handheld IRT very close to the canopy in an almost horizontal position. Mean canopy temperature was obtained by taking the average of eight readings taken from the eight major compass directions. Mean background temperature was obtained by taking the average of several readings taken from different points on the ground with no foliage in the instrument field of view. Air temperature was also monitored by another sensor in the Scheduler. All measurements were replicated twice.

Field checking of the instruments was done by comparing the IRT readings to a blackbody calibration source (Everest 1000, Everest Interscience, Inc.) before and after each set of readings. The IRTs were also calibrated in the laboratory before and after the experimental period. There were no significant changes observed in the calibrations.

Measurements were made on clear days or during periods when no clouds obscured the sun. It took about five minutes to finish each set of readings. All measurements were made during mid-day, 1200-1500h. This time is considered optimum for many remotely-sensed temperature applications (Gardner et al. 1981; Millard et al., 1978).

Plant parameters measured were leaf area index (LAI) and gap fractions (PGAPΘ) and canopy heights. LAI and PGAPΘ were measured using the LiCor Plant Canopy Analyzer (LAI 2000, LiCor Inc., Lincoln, NE). This instrument consists of an optical sensor and a control unit. The sensor is made of five concentric rings of radiation detectors. The lenses in front of the detectors cause the five rings to see different portions of the sky. The sensor has a filter that rejects light greater than 0.490 μm, thus minimizing the light reflected and transmitted by the leaves from reaching the detectors. The control unit records light readings above and below the canopy and calculates LAI and PGAPΘ from light interception measurements.

Data gathered throughout the experiment are presented in Tables 4.1, 4.2 and 4.3. Table 4.1 presents the grassland management practices (Treatments), percent ground cover (GC), LAI and canopy height. Table 4.2 presents the gap fractions (PGAPΘ) for the four view zenith angles. Leaf area index ranged from 0.66 to 3.81 while gap fraction at nadir ranged from 0.17 to 0.86. Canopy height ranged from 15

to 65 cm. Table 4.3 presents temperature measurements made on each plot. The measurements were made on different days with different weather conditions with air temperature ranging from 297 to 315K during the time of measurement. Canopy temperature ranged from 295 to 314K while background temperatures ranged from 307 to 332K.

From the 14 plots, four plots (Plots 2, 4, 13 and 16), representing the range of ground cover conditions for the experimental plots, were selected for use in the subsequent discussions and model development. Plot 2 was the sparsest (25% ground cover) while Plot 13 had greater than 86% ground cover. Plots 4 and 16 had intermediate ground cover of 45 and 58%, respectively. Plots 2 and 4 had relatively moist soil surface while Plots 13 and 16 were relatively dry. Data from the remaining nine plots served to validate the model.

In this study it is assumed that the mean of composite temperature readings taken at different zenith view and azimuth angles represented the temperature of partially vegetated surfaces. The mean composite temperature (Tm) for each plot was obtained by taking the average of 33 readings taken from different view zenith angles and azimuthal directions. Then, the composite temperature reading for each zenith view angle ($T\Theta$) was divided by Tm thus, transforming the data into relative values (Tr) with respect to the mean (i.e., $Tr=T\Theta/Tm$). This normalizing procedure made the data comparisons easier.

5.3 Results and Discussions

A graph of Tr against zenith view angle for four selected plots is shown in Fig. 5.1 A striking feature observed in Fig. 5.1 is the convergence of the lines towards the 40° view angle and a relative temperature of 1.0. Data to the left of 40° view angle

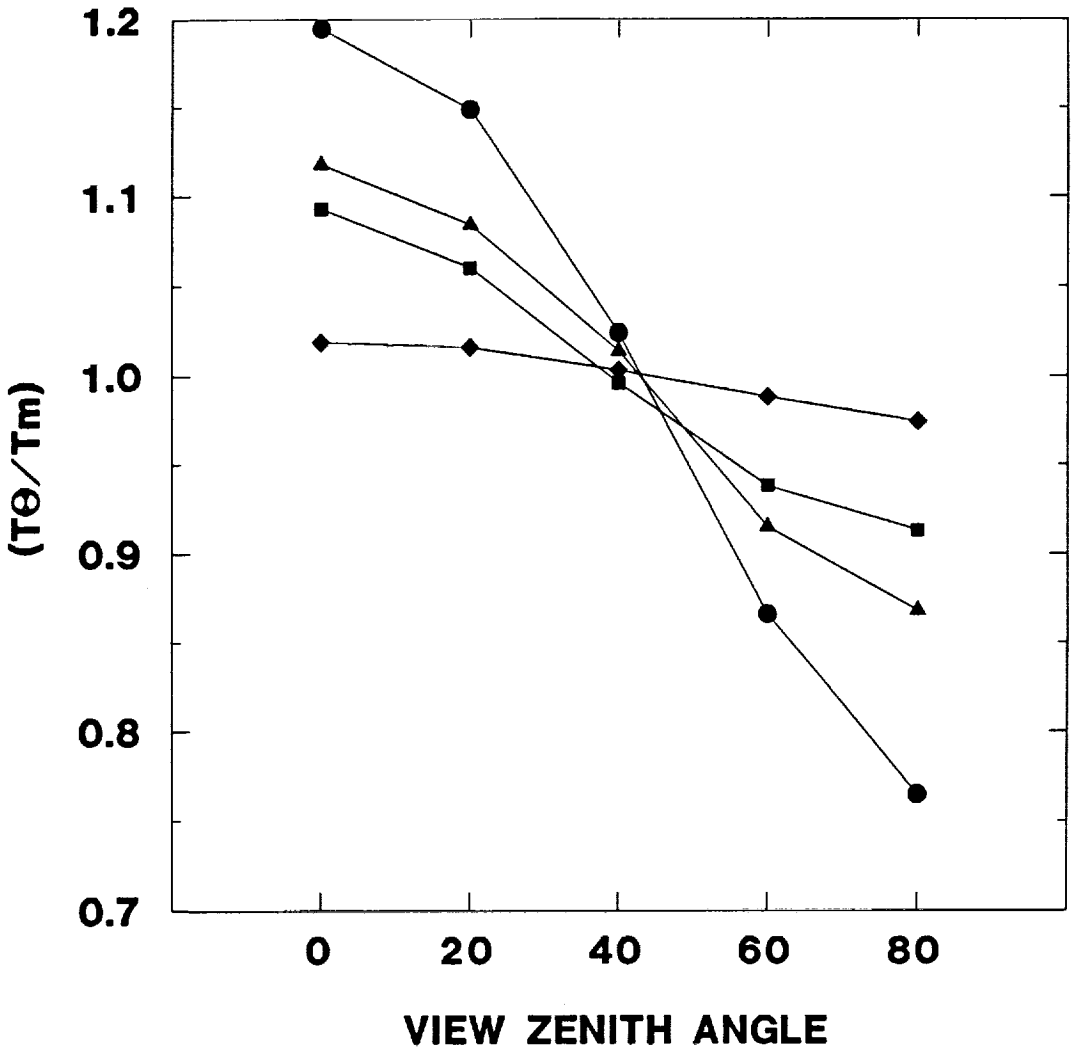

Figure 5.1. Variation of composite temperature (TΘ) relative to the mean surface temperature (Tm) for the different plots (●)P2, (▲)P4, (■)P16 and (♦)P13.

had relative temperatures greater than 1.0 indicating a surface temperature higher than Tm. The reverse is true for data to the right of 40° view angle. The relative deviation from Tm (i.e., |Tr-1|) increases as the view departs from the 40° view angle with maximum deviation at the two extreme zenith view angles. Deviations are large for sparse canopies and small for canopies with almost full cover. At the 40° view angle the surface temperature is close to the mean i.e. Tr=1.0. This suggests

that the mean temperature can be obtained by viewing the surface from or near a 40° zenith angle. At this angle the canopy and the background are presented to the instrument in more or less equal proportions (Table 4.3). At view angles less than 40°, the proportion of the background increases while that of the canopy decreases. Since the background often has a higher temperature than the canopy, the composite temperature is higher than the mean. The reverse is true for view zenith angles greater than 40°.

The significance of Tm as the representative composite temperature of partially vegetated surfaces can be judged from the following corroborative studies: Blad et al. (1990) compared the measured outgoing longwave radiation and sensible heat flux with those estimated from composite temperature measurements taken from different view zenith angle. They concluded that reasonable estimates of outgoing longwave radiation and sensible heat flux can be obtained from composite temperatures measured at the 40° view zenith angle. Brunel (1989) used remotely-sensed composite temperatures measured at 45° view zenith angle to estimate evapotranspiration and reported good agreement between the estimated and measured values. Moran et al. (1989) reported that composite temperature measured from nadir overestimated the aerodynamic temperature. Huband and Monteith (1986) compared radiative crop temperatures measured at 55° zenith view angle with aerodynamic temperatures estimated from profiles of temperature and wind speed and concluded that the composite temperature was consistently 1.0 K lower than the aerodynamic temperature. Hatfield et al. (1984) used remotely-sensed temperatures measured from a view zenith angle of 60° to estimate sensible heat flux and reported that it underestimated the composite temperature. The above citations

suggest that use of radiometric temperatures obtained from view zenith angle other than 40° or 45° for radiation and energy balance studies overestimated/ underestimated the actual values while those taken from or near the 40° view zenith angle closely approximated the actual values. From the above findings and those of this study it is reasonable to conclude that Tm is the representative temperature to use for estimating longwave radiation or sensible heat flux using remote sensing techniques.

From Fig. 5.1 it is evident that the mean surface temperature will be overestimated or underestimated by as much as 20% depending on the degree of ground cover and viewing angle. This translates into an error of about 6°C for a surface temperature of 30°C. An error of this magnitude can lead to an error of more than 250 W/m² in H (Moran et al., 1989).

Modeling the Mean Surface Temperature. The relative deviation of the sensor temperature response (Trm), i.e.,

$$(Trm=(T\Theta^4-Tm^4)/Tm^4) \qquad (5.4)$$

was calculated for the different view zenith angles. A scatter plot of Trm with PGAPΘ is shown in Fig. 5.2. When TΘ was measured at 40°view zenith angle, the relative deviation remained very close to 0 regardless of canopy gap fraction. For view zenith angles less than 40°, Trm increased with increasing gap fractions while for angles greater than 40° it decreased.

For measurements taken at view zenith angles of 0° and 20° a direct linear relationship between Trm and PGAPΘ was apparent (Fig. 5.2). The model

$$Trm = 0.106PGAP\Theta \qquad (5.5)$$

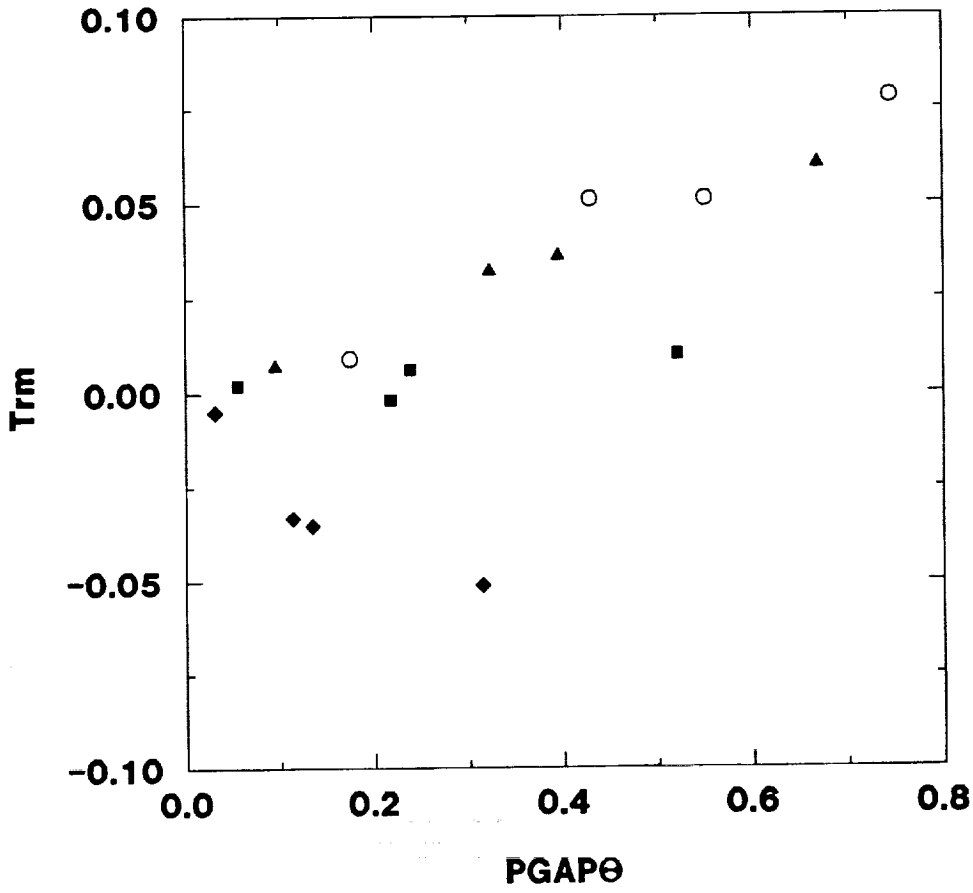

Figure 5.2. Scatter plot of Trm versus PGAPΘ for the different view zenith angles (○)0°, (▲)20°, (■)40° and (◆)60°.

was fit to the data. About 95% of the variation in Trm can be explained by the variation in PGAPΘ (Fig. 5.3). The mean composite temperature, Tm, can thus be calculated as:

$$Tm = T\Theta(1.0 + 0.106PGAP\Theta)^{-0.25} \quad (5.6)$$

where TΘ refers to a 0° or 20° reading.

For measurements taken at 60°, a negative linear relationship exists between Trm and PGAPΘ (Fig. 5.4). The model:

$$Trm = -0.009 - 0.146PGAP\Theta \quad (5.7)$$

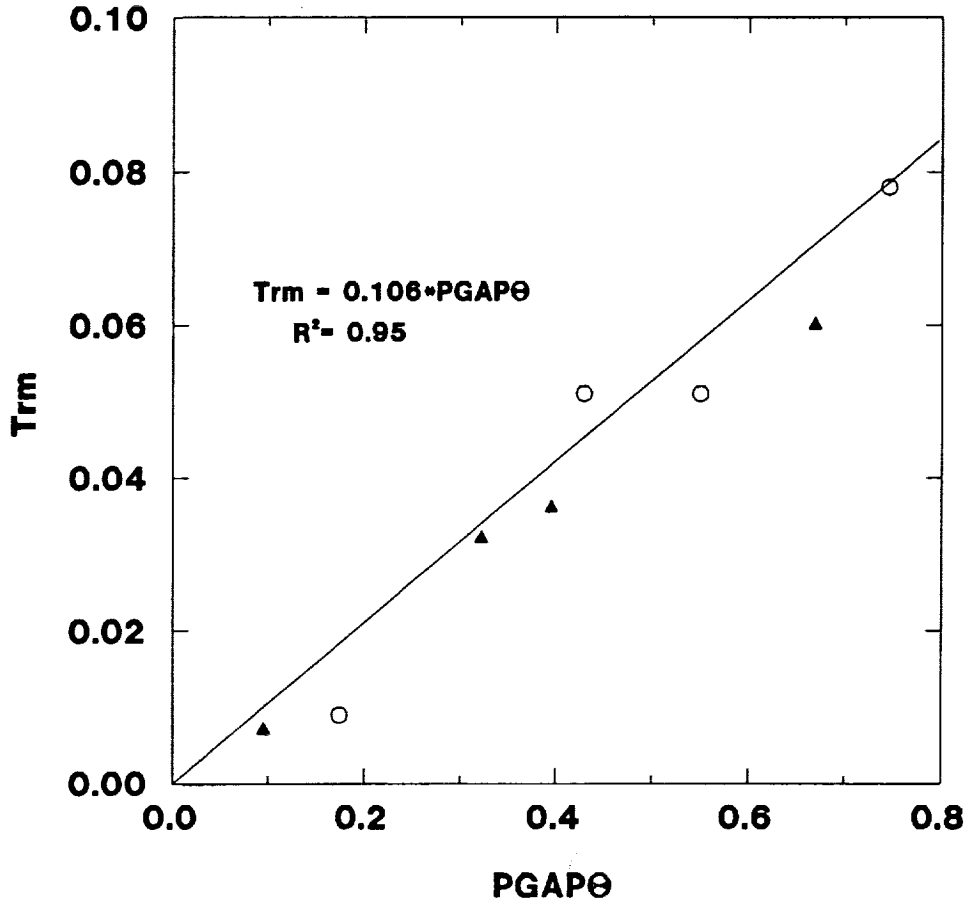

Figure 5.3. Relationship of Trm taken from nadir (○) and 20° (▲) view zenith angle to PGAPΘ. The solid line is the equation Trm = 0.106PGAPΘ.

was fitted to the data with an $r^2 = 0.83$. Tm can be calculated as:

$$Tm = T60(0.991 - 0.146PGAP\Theta)^{-0.25} \quad (5.8)$$

Equations 5.6 and 5.8 were applied to the data of the remaining nine plots acquired in this study. A comparison of the Tm estimated using Eqs. 5.6 and 5.8 with the observed values is shown in Figs. 5.5 and 5.6, respectively. Good agreement was obtained with a RMSE of 0.39 for both models.

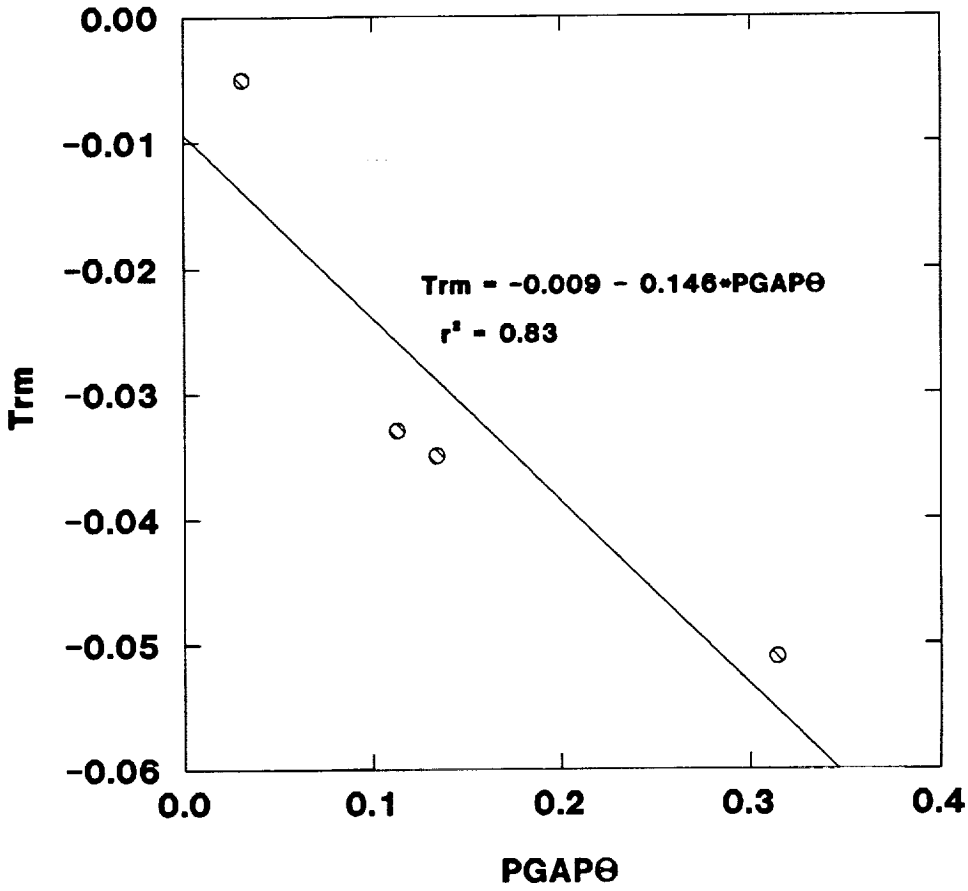

Figure 5.4. Relationship of Trm measured from 60° view zenith angle to PGAPΘ. The solid line is the equation Trm = -0.009 - 0.146PGAPΘ.

5.4 Summary and Conclusions

The dependence of remotely-sensed surface temperature on viewing angle and direction has been observed in many studies, but the question of which of the directional temperature measurements should be used for a given application has not been fully addressed. Results of this study suggest that the mean composite temperature may represent the surface temperature used to estimate sensible heat flux and emitted longwave radiation from partially vegetated surfaces. Mean composite temperature (Tm) can be obtained by viewing the surface from a zenith

angle of about 40°. Temperatures observed at other view angles can differ from Tm by as much as 20%, depending on the percentage of ground cover and zenith view angle. Tm can be estimated from remotely-sensed temperature measured from various view zenith angles with the models:

$$Tm = T\Theta(1.0 + 0.1055PGAP\Theta)^{-0.25}$$

for measurements taken at view zenith angles less than 40° and:

$$Tm = T60(0.993 - 0.1461PGAP\Theta)^{-0.25}$$

for temperatures taken at 60° view zenith angle.

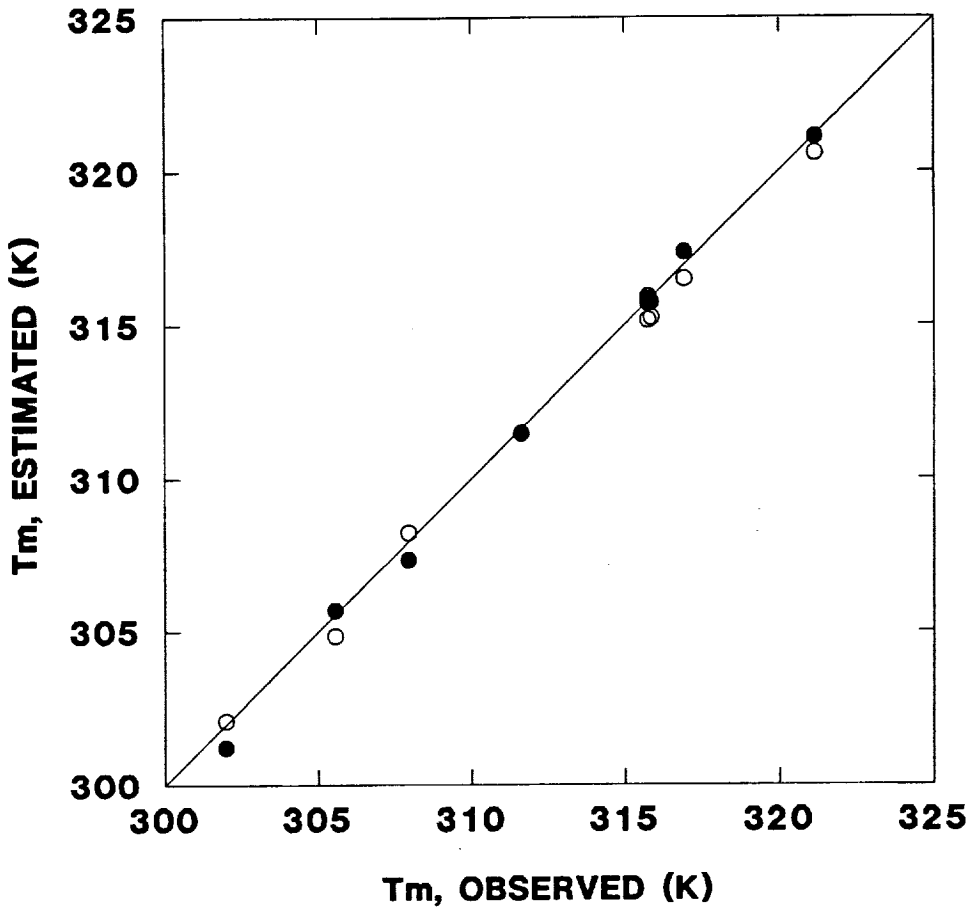

Figure 5.5. Comparison of mean temperature (Tm) estimated from $Tm=T\Theta(1.0+0.106PGAP\Theta)^{-0.25}$ with observed values for the (○)nadir and (●)20° view zenith angles.

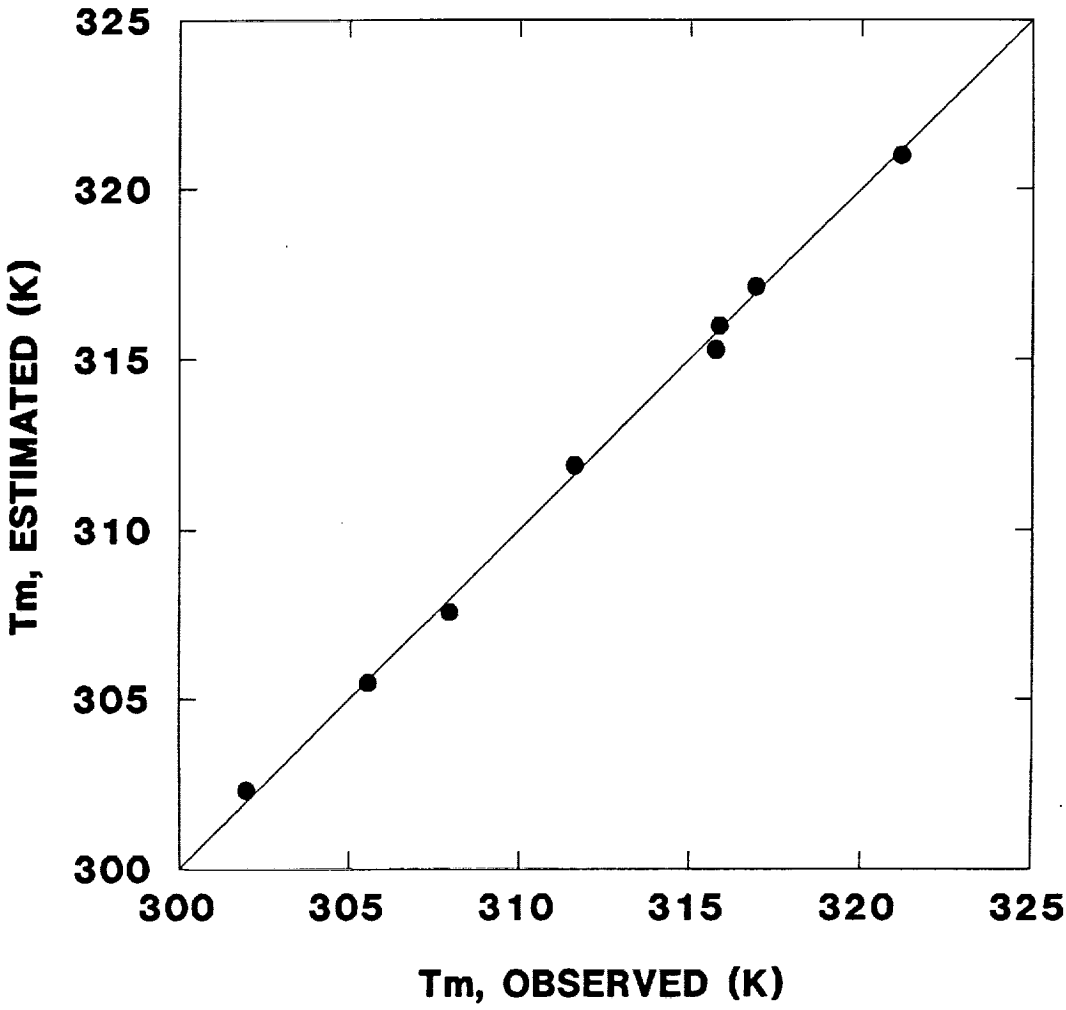

Figure 5.6. Comparison of Tm estimated from $Tm=T60(0.991-0.146PGAP\Theta)^{-0.25}$ with observed values. The solid line is the 1:1 line.

6. Estimating Gap Distribution in Partially Vegetated Surfaces from Remotely-Sensed Information

6.1 Introduction

The probability of gap (PGAPΘ), defined as the probability that a beam of radiation will pass through a canopy uninterrupted and hit the background at a point is an important parameter in remotely sensing the temperature of the components (canopy and soil) of partially vegetated surfaces. It greatly influences the signal reaching the remote sensor as demonstrated in the Secs. 4.0 and 5.0 and in the studies of Kimes (1980), Heilman et al. (1981), Norman and Welles (1983), Kimes et al. (1985), Matthias et al. (1987) and Sobrino and Caselles (1990). PGAPΘ is a complex function of the distribution and density of plants, leaf area index and leaf angle distribution and varies with viewing angle and direction.

The gap distribution in plant canopies may be estimated using photographic techniques or by direct measurement (e.g., using a Licor LAI 2000, LiCor, Inc., NE). These techniques are probably inadequate to meet the gap distribution data needed to estimate the canopy temperature over large areas. The most common way of solving for PGAPΘ is to treat the vegetation in terms of certain geometrical shapes that can be mathematically described (Jackson et al. ,1979; Norman and Welles, 1983). However, the parameters are difficult to quantify because natural surfaces are complicated targets.

Remote sensing may be used to estimate gap fractions or PGAP in the canopy. Goel (1988) reviewed several canopy reflectance models that may be used for estimating biophysical parameters by inversion technique. The inversion technique, however, requires multiple view angles. It is not yet economically feasible

to obtain instantaneous reflectance data from several view azimuth and zenith angles using aircraft or spacecraft (Jackson et al., 1990).

Several vegetation indices (e.g., Normalized Difference Vegetation Index (NDVI), Ratio of NIR to RED, and others) have been used to relate agronomic variables to reflectance measurements (Pearson and Miller, 1972; Wiegand et al., 1974; Gardner et al., 1985). Most formulae are based on ratios or linear combinations of reflectance in different wavebands and exploit differences in the reflectance patterns of green vegetation and other objects. Simple empirically based models to estimate gap fraction at nadir/near-nadir (i.e., percent ground cover) from remotely-sensed information are available but models for estimating the angular distribution of gap are lacking. The development of pointable and off-nadir viewing sensors makes it desirable to model the angular distribution of gaps in plant canopies. The objective of this study is to develop a method for estimating the angular distribution of gaps in plant canopies using remotely-sensed information for use in remote sensing of the canopy temperature of partially vegetated surfaces.

6.2 Materials and Methods

The data used in this study were obtained from two experiments that were conducted in 1989 at the Konza Prairie near Manhattan, Kansas (Blad et al., 1990) and in 1990 at the University of Nebraska Agricultural Reasearch and Development Center, Mead, Nebraska (Cornell, 1991). The data sets include canopy bidirectional reflectance factors (RFs), leaf area index (LAI), gap fractions (PGAPΘ), mean tilt angle (MTA) and canopy height.

Bidirectional reflectance factors were derived from reflectance measurements obtained with a Barnes 12-1000 Modular Multiband Radiometer (MMR). The MMR

produces a voltage proportional to the scene radiance in seven wavelength bands from visible to middle infrared and one in the thermal infrared region. A highly reflective molded halon panel was used as a reference panel. Reflectance factors were calculated using the procedure described by Robinson and Biehl (1979).

In 1989 measurements were made at two different sites (sites 916 and 906) of the First International Land Surface Climatology Project Field Experiment (FIFE). There were five vegetated plots and one bare plot at each site. Dominant vegetation species in each plot were big bluestem (*Andropogon gerardii* Vitnam), switchgrass (*Panicum virgatum* L.) and indian grass (*Sorghastrum nutans* (L) Nash). At site 916 (Grass1) measurements were made on days 216 and 220 and at site 906 (Grass2) on days 218 and 219. Reflectance measurements were made from seven view zenith angles (-50°, -35°, -20°, 0°, 20°, 35°, and 50°) in the solar principal plane.

The 1990 experiment was conducted in an irrigated alfalfa (*Medicago sativa* L.) field. The soil was a Sharpsburg silty clay loam. Reflectance factors were obtained with the MMR from 11 view zenith angles at 10° intervals from -50° to 50° in the solar principal plane. Measurements were made over four plots on 18 days from May through September, encompassing three cutting cycles of alfalfa.

Leaf area index (LAI), gap fraction distribution (PGAPΘ), and mean tilt angle (MTA) were measured with a LiCor LAI 2000. This instrument consists of an optical sensor and a control unit. The sensor is made of five concentric rings of radiation detectors. The lenses in front of the detectors cause the five rings to see different portion of the sky. The sensor has a filter that rejects light greater than 0.490 μm, thus minimizing the light reflected and transmitted by leaves from reaching the

detectors. The control unit records light readings above and below the canopy and calculates LAI, PGAPΘ and MTA from light interception measurements at five angles.

Reflectance data collected at mid-day (1200-1500h) in the red (0.630-0.690μm) and near infrared (0.760-0.900μm) wavelength bands corresponding to MMR channel 3 (CH3) and MMR channel 4 (CH4) were used in this study. The two bands were chosen for their contrasting reflectance characteristics over soil and vegetation. Reflectance factors in these two channels were used to compute the ratio (SRΘ)

$$SR\Theta = CH4/CH3 \tag{6.1}$$

and the logarithm of the ratio (LRΘ)

$$LR\Theta = Ln(CH4/CH3) \tag{6.2}$$

6.3 Results and Discussions

Table 6.1 presents leaf area index, average height of vegetation and mean tilt angle (leaf inclination angle) for five plots of each cover type, i.e., GRASS1, GRASS2 and ALFALFA. There was a very limited range of LAI for the grass plots ranging from 1.68 to 2.37 for GRASS1 and 1.51 to 2.45 for GRASS2. A wider range of LAI was measured for ALFALFA plots from 0.41 to 4.57. The plot number for ALFALFA refers to a day of measurement and the data represent the mean of the measurements from different areas made during the day. Gap fraction distributions for the three cover types are shown in Figs. 6.1-6.3. In the subsequent discussions, comparisons made between each cover type will refer to plots with about the same LAIs.

Table 6.1. Leaf Area Index (LAI), canopy height (HGT) cm. and mean tilt angle (MTA) of the different plots.

	GRASS1			GRASS2			ALFALFA		
PLOT	LAI	HGT	MTA	LAI	HGT	MTA	LAI	HGT	MTA
1	2.03	20	65	1.59	33	61	4.57	68.7	43
2	2.22	25	61	1.51	30	58	0.80	16.3	60
3	2.07	35	59	2.45	39	46	1.39	36.7	50
4	2.37	40	62	1.80	28	59	2.29	42.5	48
5	1.68	25	67	1.98	32	56	0.41	11.9	67

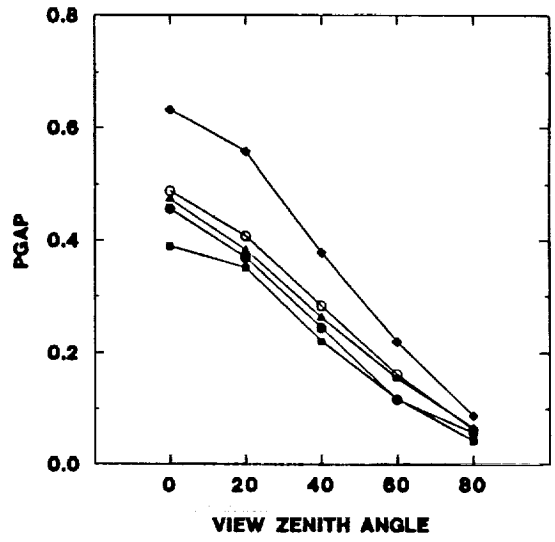

Figure 6.1. Angular distribution of gaps for Grass1 plots (○)P1, (●)P2, (▲)P3, (■)P4, (◆)P5.

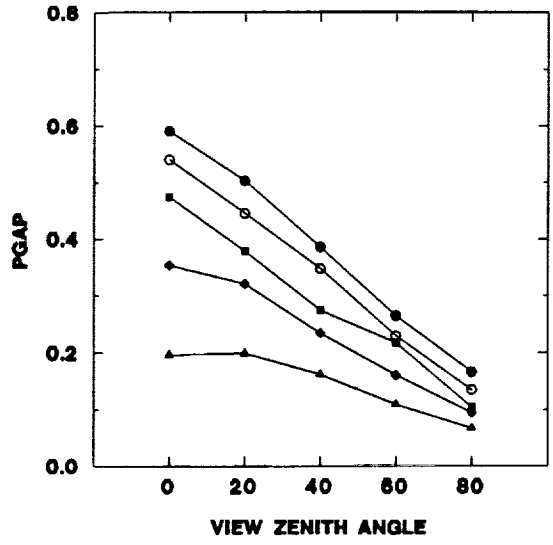

Figure 6.2. Angular distribution of gaps for Grass2 plots (○)P1, (●)P2, (▲)P3, (■)P4 and (◆)P5.

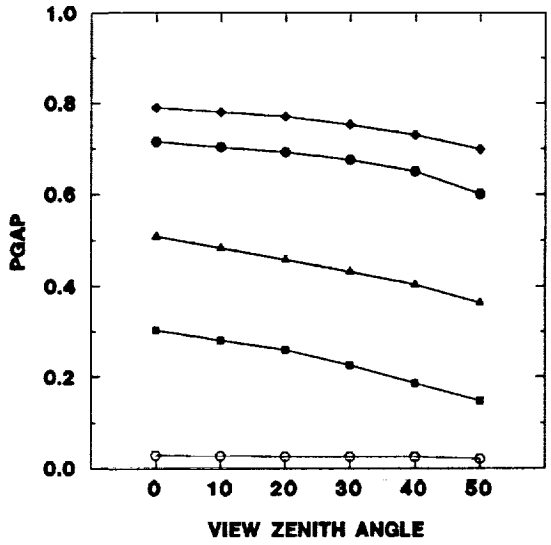

Figure 6.3 Angular distribution of gaps for Alfalfa plots (○)P1, (●)P 2, (▲)P3, (■)P4, and (◆) P5.

Trends in Reflectance Patterns in Channel 3. Trends in bidirectional reflectance patterns for CH3 are shown in Figs. 6.4, 6.5, and 6.6. A curve for the bare soil reflectance is included in Fig. 6.4 for comparison. The dips at (-35°) of Fig. 6.4 and at (-20°) of Fig. 6.5 could be due to the shadow of the instrument. Directional reflectance patterns of partially vegetated surfaces showed approximately the same trends as the bare soil reflectance. That is, reflectance decreased in the forward scatter direction (away from the sun) and increased in the back scatter direction (towards the sun) with a peak at about 20-40° in the backscatter direction. Alfalfa plots showed the least variation in reflectance with view angle followed by Grass2 and Grass1 plots. For all plots reflectance decreased with increasing ground cover.

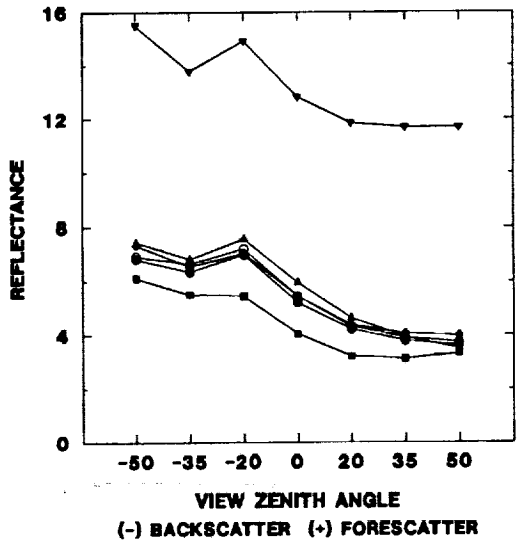

Figure 6.4. Percent reflectance for CH3 as function of view zenith angle for Grass1 plots (○)P1, (●)P2, (▲)P3, (■)P4, (◆)P5 and (▼)Soil. Solar zenith angle is 33°.

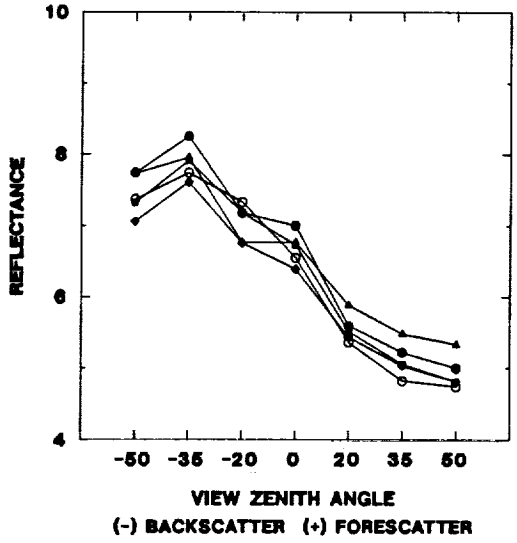

Figure 6.5. Percent reflectance in CH3 as a function of view zenith angle for Grass2 plots (○)P1, (●)P2, (▲)P3, (■)P4 and (◆)P5. Solar zenith angle is 23°.

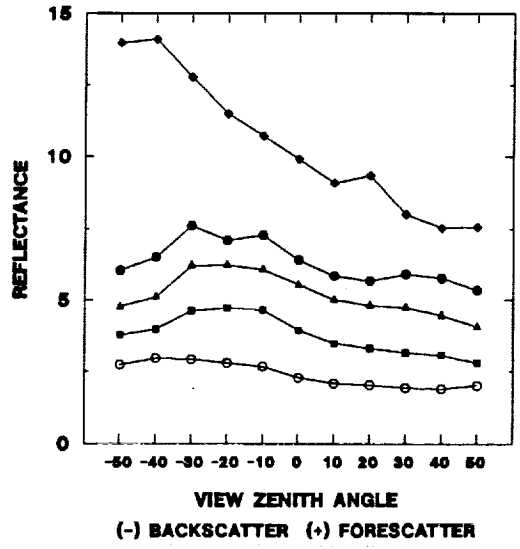

Figure 6.6. Percent reflectance in CH3 as a function of view zenith angle for Alfalfa plots (○)P1, (●)P2, (▲)P3, (■)P4 and (◆)P5. Solar zenith angle ranged from 17-35°.

Differences in trends in the forescatter and backscatter directions are due to differences in illumination condition of the canopies in these two directions. As the view angle is increased in the forescatter direction, more shaded components come into view of the instrument causing a decrease in the overall reflectance. In the back scatter direction, the strong back scattering characteristic of soil and vegetation caused an increase in reflectance.

Differences in the magnitude of response to increasing view zenith angle between each cover types can be explained by the changes in the proportion of the soil and vegetation that is viewed by the sensor (Figs. 6.1, 6.2 and 6.3). For alfalfa plots the proportion of ground viewed by the sensor changes very little with view angle compared to Grass1 and Grass2 plots that had more or less the same LAI as alfalfa. Thus, the contribution of the soil to the overall reflectance changed very little for alfalfa, while for Grass1 and Grass2 the contribution of the soil greatly diminished as the view zenith angle increased.

Reflectance Patterns in Channel 4. Trends in reflectance patterns for channel 4 differed for each type of vegetation (Figs. 6.7, 6.8 and 6.9). Grass1 showed an increase in reflectance in both the forward and backscatter direction from a minimum near nadir. Grass2, on the other hand, showed a marked increase in reflectance in the backscatter direction and a slight tendency for decrease reflectance in the forwardscatter direction with a minimum at about 20°. Alfalfa decreased in reflectance from the backscatter to the forward scatter direction with a minimum at about 30° to 40°.

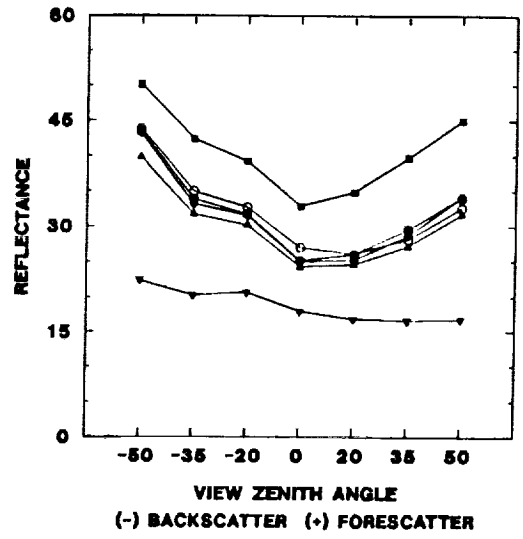

Figure 6.7. Percent reflectance in CH4 as a function of view zenith angle in the solar principal plane for grass1 plots (○)P1, (●)P2, (▲)P3, (■)P4, (♦)P5 and (▼)Soil. Solar zenith = 33°.

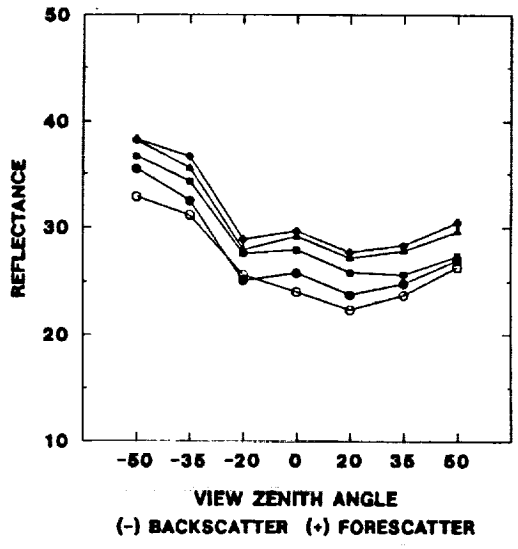

Figure 6.8. Percent reflectance in CH4 as function of view zenith angle in the solar pricipal for Grass2 plots (○)P1, (●)P2, (▲)P3, (■)P4, (♦)P5. Solar zenith angle is 23°.

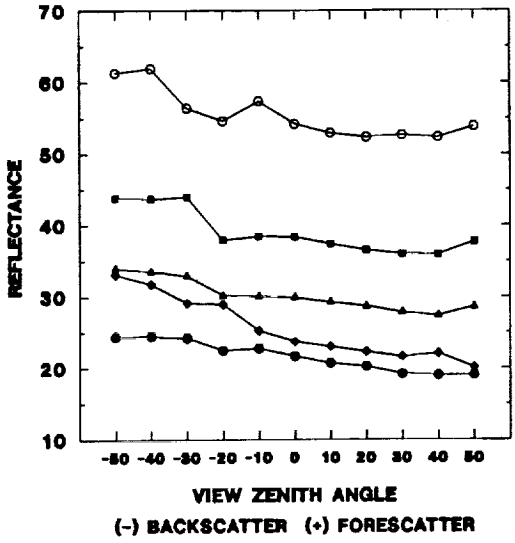

Figure 6.9. Percent reflectance in CH4 as a function of view zenith angle in the solar principal plane for Alfalfa plots (○)P1, (●)P2, (▲) P3, (■)P4 and (♦)P5.

Differences in reflectance pattern trends in the forescatter direction can be explained by the differences in the geometric structure (mean tilt angle) of each types of vegetation (Table 6.1). Canopies with more vertical components (indicated by higher mean tilt angle) allow deeper penetration of radiation into the canopy (less shading) than do canopies with more horizontal components. In the forescatter direction the portion of shaded components viewed by the sensor increases as the off-nadir view angle increased. This results in lower reflectance. This shading effect can be off-set by another mechanism explained as follows: In the NIR bands, vegetation canopies are characterized by high reflectance and high transmittance. For canopy structures with more vertical components the underside of the leaves are viewed by the sensor as the off-nadir view is increased. Since canopies have high transmittance in the NIR band, some of the radiation transmitted through the leaves can reach the sensor directly resulting into a higher signal recorded by the instrument. This effect

is observed at viewing angles greater than the leaf inclination angles.

RATIO (CH4/CH3). Ratios of CH4/CH3 for the different cover types are shown in Figs. 6.10, 6.11, and 6.12. Compared to the individual bands the ratio showed a very definite pattern. It increased with increasing off-nadir view angle. The scattering effect of the soil appears to cancel out as suggested by the nearly constant ratio for the bare soil. The anisotropic scattering properties of the canopies are still apparent as indicated by the asymmetry in the forescatter and backscatter directions. The response to changing view angle differed for each type of vegetation. Alfalfa showed the least response while Grass1 showed the greatest change with viewing angle. For each cover type the ratio increased with increasing amount of vegetative cover.

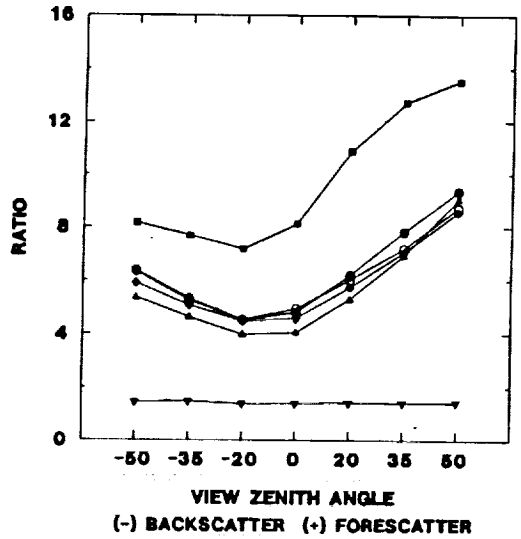

Figure 6.10. Ratio of CH4/CH3 as a funciton of view zenith angle in the solar principal plane for Grass1 plots (○)P1, (●)P2, (▲)P3, (■)P4, (◆)P5, (▼)Soil.

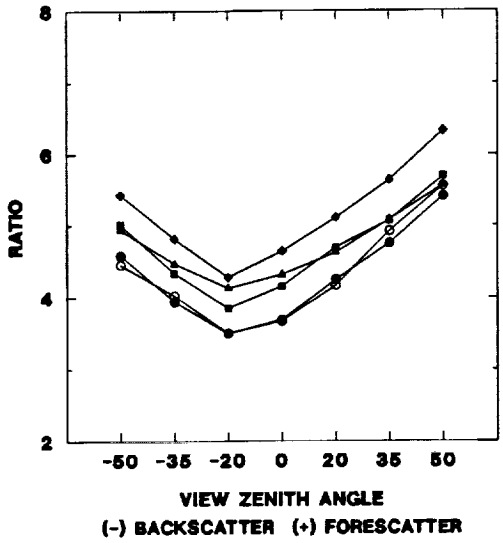

Figure 6.11. Ratio of CH4 to CH3 as a function of view zenith angle in the solar principal plane for Grass2 plots (○)P1, (●)P2, (▲)P3, (■)P4 and (◆)P5.

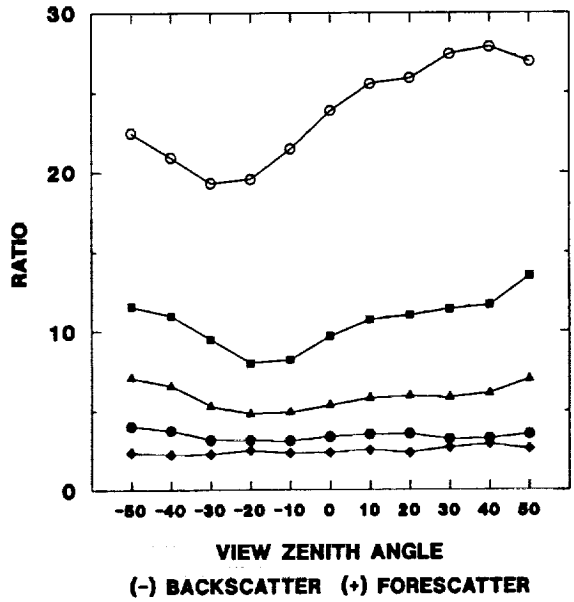

Figure 6.12. Ratio of CH4/CH3 as a function of view zenith angle in the solar principal plane for Alfalfa plots (○)P1, (●)P2, (▲)P3, (■)P 4 and (◆)P5.

Relationship of PGAPθ to Reflectance Factors (RF) and Ratio (Ch4/CH3). As the sensor is moved from nadir to off-nadir view angles the proportion of soil in the field of view of the instrument is decreased. In spectral bands where the soil is more reflective than the vegetation (e.g., infrared) one expects the overall reflectance to decrease with increasing view angle. The reverse is true for wavelength bands in which the canopy reflects strongly (e.g., near infrared). The anisotropic scattering properties of the soil significantly influence the observed directional reflectance in the visible band and tend to dominate the reflectance distribution for sparse canopies.

From reflectance pattern trends for the individual bands it appears that there is no definite relationship between RFs and PGAPθ. The ratios of CH4 to CH3 have a definite relationship to PGAPθ by virtue of PGAP's relationship to view angle. From the view angle responses, however, it follows that there will be a different relationship between the ratio and PGAPθ which depends on the cover type.

The relationship between the CH4/CH3 ratio and PGAPθ is presented in Fig. 6.13. Due to a very limited range of LAI sampled for grass plots, only the data for alfalfa are shown. Because of differences in response in the backscatter and forescatter directions, the plotted points were designated as measured from the forescatter or backscatter directions. The ratio exhibited a negative exponential relationship with PGAPθ as shown by the equation,

$$PGAP\theta = 1.115\exp(-0.154SR\theta) \qquad (6.3)$$

($r^2 = 0.98$). A slightly different equation was developed for each view direction. The equations,

$$PGAP\theta = 1.134\exp(-0.164SR\theta) \quad (6.4)$$

with $r^2=0.97$ and

$$PGAP\theta = 1.096\exp(-0.144SR\theta) \quad (6.5)$$

with $r^2=0.98$ fit the data for the backscatter and forescatter directions respectively.

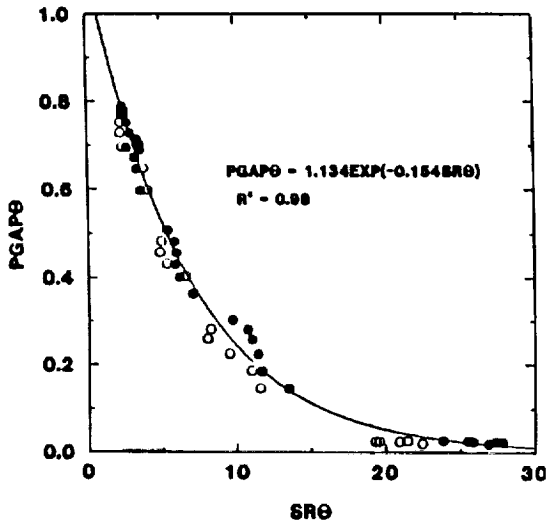

Figure 6.13. Relation ship of PGAPθ to ratio (SRθ). The symbols (○) and (●) refer to data taken from the backscatter and forescatter directions respectively.

The logarithm of the ratio (LRθ) on the other hand showed a strong linear relationship with gap (Fig. 6.14). The equation,

$$PGAP\theta = 1.052 - 0.333LR\theta \quad (6.6)$$

fitted the entire data set with $r^2=0.97$. For the backscatter and forescatter directions, the equations

$$PGAP\theta = 1.058 - 0.346LR\theta \quad (6.7)$$

with $r^2=0.97$ and

$$PGAP\theta = 1.059 - 0.324*LR\theta \quad (6.8)$$

with $r^2=0.98$ fitted the data for the forwardscatter and backscatter directions, respectively.

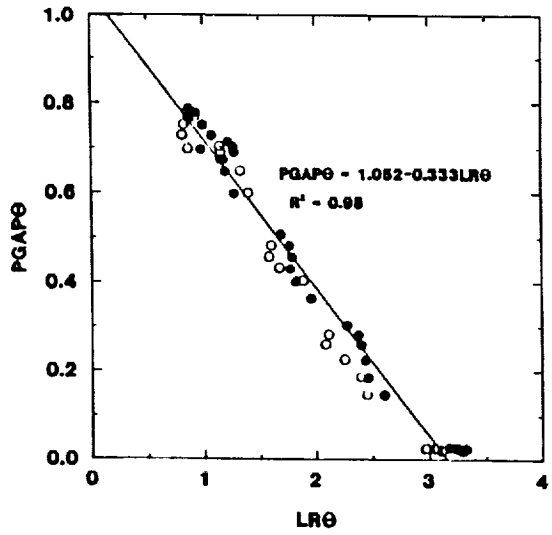

Figure 6.14. Relationship of PGAPΘ to the logarithm of the ratio (LRΘ). The symbols (○) and (●) refer to data taken in the backscatter and forescatter directions respectively.

Equations 6.3 and 6.8 were applied to the remaining 13 alfalfa plots. Comparison of the measured PGAPΘ with the estimated values using the SRΘ and the LRΘ models are shown in Figs. 6.15 and 6.16. The scatter in the data points could have been caused by the changes in soil moisture status, amount of litter on the ground and structural changes in the vegetation during the 137 days of the data gathering period. Overall, there is a fairly good agreement with a RMSE of 0.09 for both models.

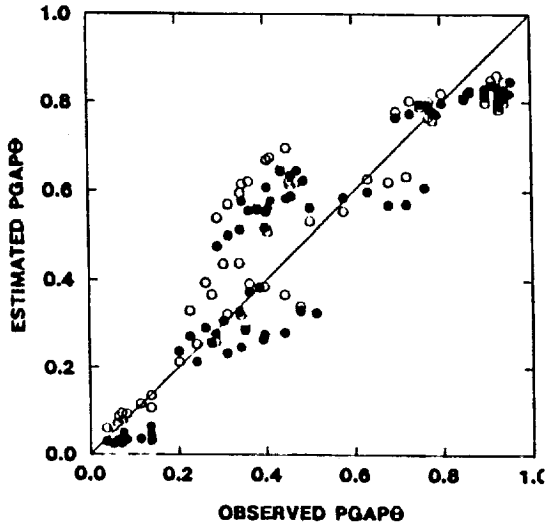

Figure 6.15. Comparison of PGAPΘ estimated from PGAPΘ=1.11exp(-0.154SRΘ) with the observed balues for the (○) backscatter and (●) forescatter directions. The solid line is the 1:1 line.

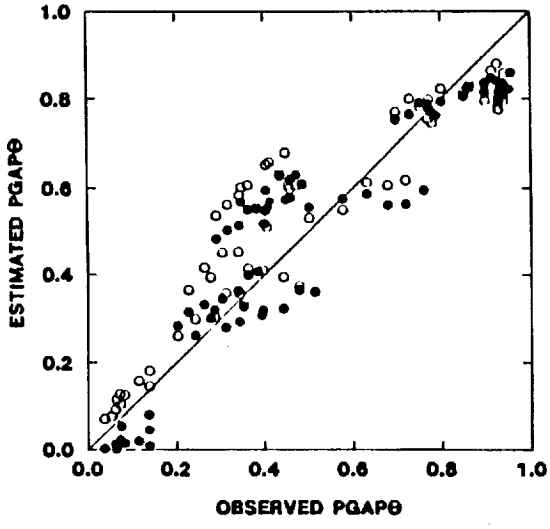

Figure 6.16. Comparison of PGAPΘ estimated from PGAPΘ=1.052-0.333LRΘ with the observed balues for the (○) backscatter and (●) forescatter directions. The solid line is the 1:1 line.

6.4 Summary and Conclusions

This study provided a good opportunity to compare the directional reflectance

patterns of surface covers which differed in geometric structure. The type of surface influenced the spectral reflectance in the forescatter and backscatter viewing directions. Alfalfa, with a planophile canopy structure was less responsive to changing zenith view angle than grass, an erectophile canopy. There was a unique relationship between the directional reflectance and view zenith angle for each cover type.

Directional reflectance patterns of sparse canopies are strongly influenced by the backscattering properties of soil. This influence can be observed even at moderate percentages of ground cover. The CH4/CH3 ratio did not seem to be influenced by the backscatter effects of the soil but, the anisotropic scattering effects of vegetation were still observed.

The ratio (SRΘ) and the logarithm of the ratio (LRΘ) exhibited a strong relationship with PGAPΘ. The high coefficient of determination (r^2) indicates that it should be possible to estimate gap distribution in plant canopies from directional reflectance measurements.

7. Summary and Recommendations

Reflectance factors tend to differ between sloped and leveled surfaces. Although various factors probably contribute to this (including species differences, vegetative cover and background cover), surface roughness and thus shadows may play an important role. More studies under controlled conditions are needed to find the significance of surface roughness on reflectances from sloped grass-cover surfaces.

The incoming shortwave component was underestimated on the average by 14 Wm^{-2} (compared to 4 Wm^{-2} in previous studies). The reflected shortwave component was overestimated by about the same magnitude as in previous studies, even though reflected radiation was measured in an azimuthal plane other than the solar principal plane. Albedo estimates were in poor agreement with measured values (10-17% MRE) compared to 4% MRE with FIFE 87-89 level sites. Large errors in incoming and reflected shortwave components contributed to the general overestimate of albedo. The cosine correction to the total incoming shortwave and the lack of coincident measurement of Eppley PSP with the MMR may be factors contributing to the overestimate. Bare soil albedos were greatly underestimated. Nadir derived estimates were in better agreement but often underestimated the measured value.

Sensible heat flux (H) estimated with remotely-sensed surface temperatures were calculated and compared to sensible heat flux values measured with micrometeorological techniques. Overall, the best estimates of H were made using canopy temperatures measured at the instrument view zenith angle of 40°. There was considerable variability, however, insofar as identifying the optimum view zenith angle with which to view the canopy at a specific time and under specific wind conditions.

Results suggested that the wind speed affected the optimum view zenith angle. Days with average wind speeds above 5 m s^{-1} coincided with the days on which the nadir and 20° view zenith angles provided canopy temperatures that resulted in the best estimates of sensible heat flux. On days with average wind speeds of less than 4 m s^{-1}, the 40° and 60°

view zenith angles provided the best estimates of sensible heat flux. Wind speed should therefore be considered when selecting the appropriate view zenith angle for measuring canopy temperature to estimate sensible heat flux over prairie grasslands.

The temperature measured by a remote sensor is a composite temperature of the surfaces (e.g., canopy and its background) exposed to the instruments. It varies with view angle and direction. In this study we addressed the problems encountered in thermal remote sensing when the surface is partially vegetated, i.e., how can one isolate the canopy temperature from the composite temperature and how does one obtain composite temperature which is representative of the surface.

Results indicated that the composite temperature ($T\Theta$) can differ from the canopy temperature (Tc) by as much as 13 K depending on the percentage of ground cover and the view zenith angle. The deviations of the composite temperature from the canopy temperature were found to be linearly related to the gap fraction ($PGAP\Theta$) along the viewing direction and exponentially related to the leaf area index divided by the cosine of the view zenith angle ($LAI/\cos\Theta$). Two models, $Tc = T\Theta*(1+0.231*PGAP\Theta)^{-0.25}$ and $Tc = T\Theta*(1+0.527*\exp(-0.804*LAI/\cos\Theta)^{-0.25}$ were developed to estimate the canopy temperature from the composite temperature. Good agreement was obtained between the estimated and observed values (RMSE < 0.56). Inputs to these two models can be acquired by remote sensing techniques. The directionality of remotely-sensed temperature was investigated to address the problem of obtaining the representative composite temperature of partially vegetated surfaces. It was assumed that the mean or average of the temperature readings taken from different azimuthal and zenith view angles would represent the temperature of partially vegetated surfaces for radiation/energy balance studies. Results indicated that the mean composite temperature can be obtained by viewing the surface from a zenith angle of about 40°. Temperatures measured from other view zenith angles can differ from the mean temperature by as much 20% depending on the view zenith angle and percentage of ground cover. Temperatures observed from view zenith angles less than 40°

overestimated the mean temperature while those observed from zenith view angle greater than 40° underestimated the mean temperature. The relative deviation of the directional temperatures from the mean was linearly related to the gap fraction along the view direction. Two models, $Tm = T\Theta*(1.+ 0.105*PGAP\Theta)^{-0.25}$ and $Tm = T60*(0.99 - 0.146*PGAP\Theta)^{-0.25}$ were developed to estimate the mean composite temperature from directional temperatures measured from view zenith angles less than 40° and from view zenith angle of 60°, respectively. Good agreement was observed between the estimated and measured values (RMSE=0.39).

Corroborative evidence obtained from the scientific literature suggests that for applications (e.g., radiation/energy balance studies) which use remotely-sensed surface temperatures as an input, better agreement between the estimated and actual values of longwave radiation or sensible heat fluxes can be obtained if the temperature used in the calculation is adjusted to the mean temperature (Tm).

The distribution of gap (PGAPΘ) in plant canopies is an important parameter in remote sensing of the surface temperature of partially vegetated surfaces. The possibility of estimating gap distribution from directional reflectance measurement was investigated to enable the predictions of canopy temperature and mean composite temperatures using remotely-sensed information as the primary input. Directional reflectance data obtained in the solar principal plane for two cover types (prairie vegetation and alfalfa) which differ in canopy structure were analyzed. Results indicated that for sparse canopies the directional reflectance in the red (0.630-0.690μm) and NIR (0.760-0.900μm) wavelength bands, corresponding to MMR CH3 and CH4 respectively, are strongly affected by the anisotropic scattering properties of the soil background and vegetation. The asymmetry of the directional reflectance patterns in the forescatter and backscatter direction suggest that the directional reflectance in the individual bands measured in the solar principal plane was not a good predictor of gap distribution. Taking the ratio of the two bands (CH4/CH3) effectively canceled out the anisotropic scattering effects of the soil background. The gap

distribution was strongly related to this ratio. The high coefficient of determination (r^2) for the PGAPθ vs. SR suggests that it is possible to estimate gaps from reflectance measurements.

The temperature models developed in this study were based on data collected from prairie vegetation and are intended for applications that require mid-day temperature measurements. Although the models are empirical, they have a theoretical basis and hence may be applied to similar cover types. For example, they can probably be applied to small grain crops which are planted or drilled in narrow rows but they may not work for crops grown in wide rows. It is recommended that the models be tested on agricultural crops and/or models developed for other surface cover types using similar procedures. Solar zenith angles other than the one used in this study should be considered in developing the models.

The validity of the mean composite temperature (Tm) as the representative temperature to use in radiation/energy balance studies of partially vegetated surfaces needs further verification and be validated through future experiments.

The estimation of gap distribution from reflectance measurements needs further study. As indicated by the results of this study, a unique relationship exists between PGAPθ and directional reflectance for each cover types. Therefore, it is recommended that models to estimate gap distribution in plant canopies be developed for other cover types, taking into consideration solar azimuth and zenith angles other than the ones used in this study.

The results of this study provide another step towards the operational use of remote measurements of surface temperature for radiation and energy balance estimates and for the use of remotely-sensed plant temperature to assess vegetative conditions.

8. References

Asrar, G., E. T. Kanemasu, and M. Yoshida, 1985. Estimates of leaf area index form spectral reflectance of wheat under different cultural practices and solar angle. *Remote Sens. Environ.*, 17:1-11.

Balick, L. K. and B. A. Hutchison, 1986. Directional thermal exitance distributions from a leafless decidous forest. IEEE Trans. Geosci. Remote Sens., GE-24:693-698.

Blad, B. L. and N. J. Rosenberg, 1976. Measurement of crop temperature by leaf thermocouple, infrared thermometry and remotely sensed thermal imagery. *Agron. J.*, 68:635-641.

Blad, B. L., E. A. Walter-Shea, P. J. Starks, R. Vining, C. J. Hays, and M. A. Mesarch, 1990. Measuring and modeling near-surface reflected and emitted radiation fluxes at the FIFE site. Agmet Progress Report, No. 90-1.

Brunel, J. P., 1989. Estimation of sensible heat flux from measurements of surface radiative temperature and air temperature at two meters: Application to determine actual evaporation rate, *Agric. For. Meteorol.*, 46:179-191.

Carlson, T. N., J. K. Dodd, S. G. Benjamin, and J. N. Cooper, 1981. Satellite estimation of surface energy balance, moisture availability and thermal enertia. *J. Appl. Meteorol.*, 20:60-87.

Cheevasuvit, F., O. Taconet, and D. Vidal-Madjar, 1985. Thermal structure of an agricultural region as seen by NOAA-7 AVHRR. *Remote Sen. Environ.*, 17:153-163.

Choudhury, B. J. and S. B. Idso, 1984. Simulating sunflower canopy temperatures to infer root-zone soil water potential. *Agric. Forest Meteorol.*, 31:69-78.

Choudhury, B. J., R. J. Reginato, and S. B. Idso, 1986. An analysis of infrared temperature observations over wheat and calculation of latent heat flux, *Agric. For. Meteorol.*, 37:75-88.

Clawson, K. L. and B. L. Blad, 1982. Infrared thermometry for scheduling irrigation of corn. *Agron. J.*, 74:311-316.

Cornell, D., 1991. Solar and view zenith angle effects on the relationship between APAR and LAI and two commonly used vegetation indices (NDVI,SRVI). Master Thesis, University of Nebraska-Lincoln, Lincon, NE 68583.

Dubayah, R., J. Dozier and F. W. Davis, 1990. Topographic distribution of clear-sky radiation over the Konza Prairie, Kansas. *Water Resources Res.* 26(4):679-690.

Dubayah, R., 1992. Estimating regional variability in net solar radiation using Landsat Thematic Mapper and digital elevation data. *Water Resources Res.* 28:2469-2484.

Deardoff, J. W., 1978. Effecient prediction of ground surface temperature with the inclusion of a layer of vegetation. *J. Geophys. Res.*, 83:1889-1904.

Fuchs, M. and C. B. Tanner, 1966. Infrared thermometry of vegetation. *Agron. J.*, 58:597-601.

Fuchs, M., E. T. Kanemasu, J. P. Kerr, and C. B. Tanner, 1967. Effect of viewing angle on canopy temperature measurements with infrared thermometers. *Agron. J.*, 59:494-496.

Gardner, B. R., B. L. Blad, D. P. Garity, and D. G. Watts, 1981. Relationships between crop temperature, grain yield, evapotranspiration and phenological development in two hybrids of moisture stressed sorghum. *Irrigation Sci.*, 2:213-224.

Gardner, B. R., B. L. Blad, D. R. Thompson, and K. E. Henderson, 1985. Evaluation and interpretation of Thematic Mapper ratios in equations for estimating corn growth parameters. *Remote Sens. Environ.*, 18:225-234.

Gardner, B. R. and B. L. Blad, 1986. Evaluation of spectral reflectance models to estimate corn leaf area while minimizing the soil background effects. *Remote Sens. Environ.*, 20:183:193.

Goel, N. S., 1988. Models of vegetation canopy reflectance and their use in estimation of biophysical parameters from reflectance data. *Remote Sens. Rev.*, 4:1-122.

Hatfield, J.L., 1979. Canopy temperatures: The Usefulness and reliability of remote measurements. *Agron. J.*, 71:889-892.

Hatfield, J. L., A. Perrier, and R. D. Jackson, 1983. Estimation of evapotranspiration at one time of day using remotely sensed surface temperatures. *Agric. Water Manage.*, 7:341-350.

Hatfield, J. L., R. J. Reginato, and S. B. Idso, 1984a. Evaluation of canopy temperature-evapotranspiration models over various crops, *Agric. For. Meteorol.*, 32:41-53.

Hatfield, J. L., E. Kanemasu, G. Asrar, R. D. Jackson, R. D. Pinter, Jr., R. J. Reginato, and Idso, S. B., 1984b. Leaf area estimates from spectral measurements over various planting dates of wheat. *Int. J. Remote Sens.*, 6:167-175.

Heilman, J. L., E. T. Kanemasu, N. J. Rosenberg, and B. L. Blad, 1976. Thermal scanner measurement of canopy temperatures to estimate evapotranspiration. *Remote Sens. Environ.*, 5:137-145.

Heilman, J. L., W. E. Heilman, and D. G. Moore, 1981. Remote sensing of canopy temperature at incomplete cover. *Agron. J.*, 73:403-406.

Huband, N. D. S., and J. L. Monteith, 1986a. Radiative surface temperature and energy balance of a wheat canopy; 1, Comparison of radiative and aerodynamic temperatures, *Boundary Layer Meteorol.*, 36:1-17.

Huband, N. D. S., and J. L. Monteith, 1986b. Radiative surface temperature and energy balance of a wheat canopy; 2, Estimating fluxes of sensible and latent heat, *Boundary Layer Meteorol.*, 36:107-116.

Idso, S. B., R. D. Jackson, W. L. Ehrler, and S. T. Mitchell, 1969. A method for determination of infrared emittance of leaves. *Ecology*, 50:388-392.

Idso, S. B., R. D. Jackson, and R. J. Reginato, 1977. Remote sensing of crop yields. *Science*, 196:19-25.

Idso, S. B., J. L. Hatfield, R. D. Jackson, and R. J. Reginato, 1979. Grain yield prediction: Extending the stress degree day approach to accomodate climatic variability. *Remote Sens. Environ.*, 8:267-272.

Idso, S. B., R. J. Reginato, J. L. Hatfield, G. K. Walker, R. D. Jackson, and P. J. Pinter, Jr., 1980. A Generalization of the stress-degree-day concept of yield prediction to accomodate a diversity of crops. *Agric. Meteorol.*, 21:205-211.

Iqbal, M., 1983. *An Introduction to Solar Radiation*. Academic Press, New York. pp. 390.

Jackson, R. D., R. J. Reginato, and S. B. Idso, 1977a. Wheat canopy temperature: A practical tool for evaluating water requirements. *Water Resour. Res.*, 13:651-656.

Jackson, R. D., S. B. Idso, R. J. Reginato, P. J. Pinter, Jr., 1977b. Canopy temperature as a crop water stress indicator. *Water Resour. Res.*, 17:1133-1138.

Jackson, R. D., R. J. Reginato, P. J. Pinter, Jr., and S. B. Idso, 1979. Plant canopy information extraction from composite scene reflectance of row crops. *Appl. Optics*, 18:3775-3782.

Jackson, R. D., 1983. Canopy temperature and crop water stress. *Adv. Irrig.*, 1:43-85.

Jackson, R. D., 1985. Evaluating evapotranspiration at local and regional scales. Proc. IEEE 73:1086-1096.

Jackson, R. D., P. J. Pinter, and R. J. Reginato, 1985. Net radiation calculated from remote multispectral and ground station meteorological data, *Agric. For. Meteorol.*, 35:153-164.

Jackson, R. D., M. S. Moran, P. N. Slater and S. F. Biggar, 1987. Field calibration of reference reflectance panel. *Remote Sens. Environ.* 22:145-158.

Jackson, R. D., P. M. Teillet, P. N. Slater, G. Fedosejevs, M. F. Jasinski, J. K. Aase, and M. S. Moran, 1990. Bidirectional measurements of surface reflectance for view angle corrections of oblique imagery. *Remote Sens. Environ.*, 32:189-202.

Kanemasu, E. T., M. L. Wesely, B. B. Hicks, and J. L. Heilman, Techniques for calculating energy and mass fluxes, in *Modification of the Aerial Environment*, edited by B. J. Barfield and J. F. Gerber, pp. 156-182, American Society of Agricultural Engineers, St. Joseph, MO, 1979.

Kimes, D. S., 1980. Effects of vegetation canopy structure on remotely sensed canopy temperature. *Remote Sens. Environ.*, 10:165-174.

Kimes, D. S., S. B. Idso, P. J. Pinter, Jr., R. D. Jackson, and R. J. Reginato, 1980a. Complexities of nadir-looking radiometric temperature measurements of plant canopies. *Appl. Optics,* 19(13):2161-2168.

Kimes, D. S., S. B. Idso, P. J. Pinter, Jr., R. J. Reginato, and R. D. Jackson, 1980b. View angle effects in the radiometric measurement of plant canopy temperatures. *Remote Sens. Environ.*, 10:273-284.

Kimes, D. S., 1981. Azimuthal radiometric temperature measurements of wheat canopies. *Appl. Optics*, 20(7):1119-1121.

Kimes, D. S., J. A. Smith, and L. E. Link, 1981. A thermal IR exitance model of a plant canopy. *Appl. Optics*, 24:623-632.

Kimes, D. S., 1983a. Remote sensing of row crop structure and component temperatures using directional radiometric temperatures and inversion techniques. *Remote Sens. Environ.*, 13:33-45.

Kimes, D. S., 1983b. Dynamics of directional reflectance factor distributions for vegetation canopies. *Appl. Optics*, 22:1364

Kimes, D. S., J. M. Norman, and C. L. Walthall, 1985. Modeling the radiant transfers of sparse vegetation canopies. IEEE Trans. Geosci. Remote Sens., 23:695-704.

Kustas, W. P., B. J. Choudhury, M. S. Moran, R. J. Reginato, R. D. Jackson, and L. W. Gay, 1987. Problems with the estimation of sensible heat flux over incomplete canopy cover with thermal infrared data, in 18th Conf. Agric. For. Meteorol. and 8th Conf. Biometeorol. and Aerobiol., September 1987, Lafayette, IN. pp 87-90.

Kustas, W. P., B. J. Choudhury, M. S. Moran, R. J. Reginato, R. D. Jackson, L. W. Gay, and H. L. Weaver, 1989. Determination of sensible heat flux over sparse canopy using thermal infrared data. *Agric. and Forest Meteorol.*, 44:197-216.

Kustas, W. P., M. S. Moran, R. D. Jackson, L. W. Gay, L. F. W. Duel, K. E. Kunkel, and A. D. Matthias, 1990. Instantaneous and daily values of the surface energy balance over agricultural fields using remote sensing and a reference field in an arid environment. *Remote Sens. Environ.*, 32:125-141.

McGuire, M. J., L. K. Balick, J. A. Smith, and B. A. Hutchison, 1989. Modeling directional thermal radiance from a forest canopy. *Remote Sens. Environ.*, 27:169-186.

McNaughton, K. G., 1988. Surface temperature and surface energy balance. In " Flow and transport in natural environment: Advances and applications" (W.L. Steffen and O.T. Deanmead, Eds.). Springer Velag, Berlin, Hiedelburg. pp. 154-159.

Markham, B. L., F. M. Wood, and S. P. Ahmad, 1988. Radiometric calibration fo the reflective bands of NS001 Thematic Mapper Simulator (TMS) and Modular Multispectral Radiometers (MMR). *SPIE Recent Advances in Sensors, Radiometers and Data Processing for Remote Sensing*, 924:96-108.

Matthias, A. D., S. R. Yates, R. Zhang, and A. W. Warrick, 1987. Radiant temperatures of sparse plant canopies and soil using IR thermometry. IEEE Trans, Geosci. Remote Sens., GE-25:516-519.

Millard, J. P., R. D. Jackson, R. C. Goettleman, R. J. Reginato, and S. B. Idso, 1978. Crop water-stress assesment using airborne thermal scanner. *Photogramm. Eng. Remote Sens. Environ.*, 44:77-85.

Monteith, J. L., 1973, *Principles of Environmental Physics*, American Elsevier, New York, pp 241.

Moran, M. S., R. D. Jackson, L. H. Raymond, L. W. Gay, and P. N. Slater, 1989. Mapping of surface energy balance components by combining Landsat Thematic Mapper and ground-based meteorological data. *Remote Sens. Environ.*, 30:77-87.

Nielsen, D. S., K. L. Clawson, and B. L. Blad, 1984. Effect of solar azimuth and infrared thermometer view direction on measured soybean canopy temperature, *Agron. J.*, 76:607-610.

Norman, J. M. and J. M. Welles, 1983. Radiative transfer in array of canopies. *Agron. J.*, 75:481-488.

Parsons, A. J., 1985. Directionality in emitted infrared radiation from grassy surfaces. *Int. J. Remote Sens.*, 6:903-910.

Paw U, K. T., S. L. Ustin, and C. A. Zhang, 1989. Anisotropy of thermal infrared exitance in sunflower canopies. *Agric. Forest Meteorol.*, 48:45-58.

Pearson, R.L. and Miller. L.D., 1972. Remote mapping of standing crop biomass for estimation of the productivity of shortgrass prairie. Eighth International Symposium on Remote Sensing of Environment, University of Michigan, Ann Arbor.

Pierce, L. L. and R. G. Congalton, 1988. A methodology for mapping forest latent heat flux densities using remote sensing. *Remote Sens. Environ.*, 24:405-418.

Price, C. J., 1982. Estimation of regional scale evapotranspiration through analysis of satellite thermal infrared data. IEEE Trans. Geosci. Remote Sens., GE-20:286-292.

Reginato, R. J., R. D. Jackson, and P. J. Pinter, Jr., 1985. Evapotranspiration calculated from remote multispectral and ground station meteorological data. *Remote Sens. Environ.*, 18:75-89.

Robinson, B. F. and L. L. Biehl, 1979. Calibration procedures for measurements of reflectance factor in remote sensing field research. Proc. Soc. Photo-optical Instrumentation Eng. *23rd Annual Tech. Symp. on Measurements of Optical Radiation*, Bellinghan, WV, pp. 16-26.

Rosenberg, N. J., B. L. Blad, and S. B. Verma, 1983. *Microclimate: The Biological Environment*, 495 pp., John Wiley, New York.

Seguin, B. and B. Itier, 1983. Using midday surface temperature to estimate daily evapotranspiration from satellite thermal IR data. *Int. J. Remote Sens.*, 4:371-383.

Smith, R. C. G., H. D. Barrs, J. L. Steiner, and M. Stapper, 1985. Relationship between wheat yield and foliage temperature: Theory and its application to infrared measurements. *Agric. Forest Meteorol.*, 36:129-143.

Sobrino, A. J. and V. Caselles, 1990. Thermal infrared radiance model for interpreting the directional radiometric temperature of a vegetated surface. *Remote Sens. Environ.*, 33:193-199.

Soer, G. J. R., 1980. Estimation of regional evapotranspiration and soil moisture condition using remotely sensed crop surface temperatures. *Remote Sens. Environ.*, 9:27-45.

Starks, P. J., B. L. Blad, E. A. Walter-Shea, J. Irons and J. Ranson, 1991a. Albedo estimates from vegetated and bare soil surfaces using bidirectional reflectance data. Special session on Hydrometeorology at the 10th Conf. on Biom. and Aerobiol. Meteorology, Amer. Meteorol. Soc., September 10-13, Salt Lake City, UT, pp. 167-169.

Starks, P. J., J. M. Norman, B. L. Blad, E. A. Walter-Shea, and C. L. Walthall, 1991b. Estimation of shortwave hemispherical reflectance (albedo) from bidirectionally reflected radiance data, *Remote Sens. Environ.*, 38:123-134.

Sutherland, R. A. and F. J. Bartholic, 1977. Significance of vegetation in interpreting thermal radiation from a terrestial surface. *J. Appl. Meteorol.*, 16(8):759-763.

Walker, G. K. and J. L. Hatfield, 1979. Test of the stress-degree-day concept using multiple planting dates of red kidney beans. *Agron. J.*, 71:967-971.

Walter-Shea, E. A., B. L. Blad, C. J. Hays and M. A. Mesarch, 1991. Remotely-sensed estimates of surface radiation balance components, APAR and spectral reflectance, *AgMet Progress Report 91-3*, Dept. of Agric. Meteorol., Univ. of Nebraska, Lincoln, NE.

Walter-Shea, E. A., B. L. Blad, C. J. Hays, M. A. Mesarch, D. W. Deering and E. M. Middleton, 1992a. Biophysical properties that affect canopy reflectance and estimates of the fraction of absorbed photosynthetically active radiation. *J. Geophys. Res.* 97:18,925-18,934.

Walter-Shea, E. A., B. L. Blad, C. J. Hays and M. A. Mesarch, 1992. Slope effects on shortwave radiation components and net radiation. AgMet Progress Report 92-1.

Walter-Shea, E. A., C. J. Hays, M. A. Mesarch, and R. D. Jackson, 1992c. An improved goniometer system for calibrating field reference-reflectance panels. *Remote Sens. Environ.* 43:1-20.

Weigand, C. L., H. W. Gausman, J. A. Cuellar, A. H. Gerberman, and A. J. Richardson, 1974. Vegetation density as deduced from ERTS-1 MSS response, Third ERTS-1 Symposium. Vol. 1.

Welles, J. M., J. M. Norman, and J. D. Martsolf, 1979. An orchard temperature model. *J. Am. Soc. Hortic. Sci.*, 104:602-610.

Willmott, C. J., 1982. Some comments on the evaluation of model performance. Bull. of the American Meteorol. Society. 63:1309-1313.

Zara, P. M., 1992. Towards large area application of remotely sensed surface temperatures, Ph.D. dissertation, Univ. of Nebr., Lincoln.